# Effect of Asymmetric Foot Placement and Reduced Weight-Bearing Asymmetry on the Sit-to-Stand Task of a Unilateral Transfemoral Amputee – A Simulation Study

Rahul Ramesh

Technische Universiteit Delft

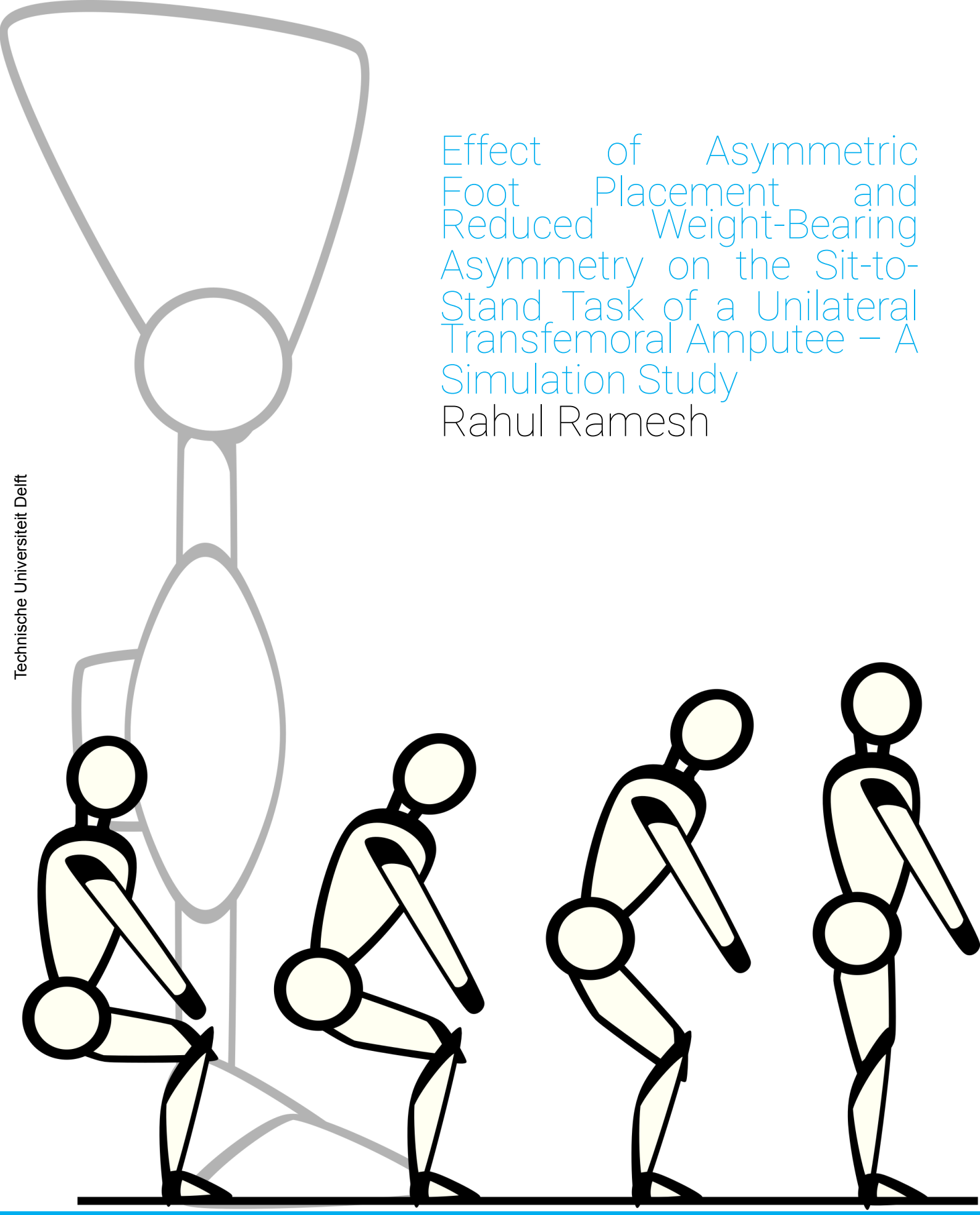

TU Delft

# Effect of Asymmetric Foot Placement and Reduced Weight-Bearing Asymmetry on the Sit-to-Stand Task of a Unilateral Transfemoral Amputee – A Simulation Study

by

Rahul Ramesh

to obtain the degree of Master of Science
at the Delft University of Technology,
to be defended publicly on Thursday November 14, 2019 at 10:45 AM.

| | | |
|---|---|---|
| Student number: | 4750284 | |
| Project duration: | April 1, 2019 – November 14, 2019 | |
| Thesis committee: | Prof. Dr. Ing. Heike Vallery, | TU Delft, Chairman |
| | Dr. Ir. Gerwin Smit, | TU Delft, supervisor |
| | Dr. Thomas Geijtenbeek, | TU Delft |

*This thesis is confidential and cannot be made public until November 14, 2022.*



TU Delft

*Let craft, ambition, spite,*
*Be quenched in Reason's night,*
*Till weakness turn to might,*
*Till what is dark be light,*
*Till what is wrong be right!*

–Lewis Carrol

# Acknowledgement

I would like to take this opportunity to express my heartful thanks to Prof.dr.ing.Heike Vallery and Dr.ir.Gerwin Smit for providing me with the opportunity to conduct my master thesis under their guidance. I am thankful for their valuable insights and their critical feedback which pushed me to my limits. I am forever grateful for their encouragement and support through my most difficult times during the thesis. I am sure that the lessons learnt while working with them will be cherished and treasured in my future endeavors. I would also like to extend my thanks to Dr.Thomas Geijtenbeek for both his support on 'SCONE' and insights towards approaching the solution to simulation problems. He has been very kind and patient in answering all of my questions.

I would like to take this opportunity to thank the entire BMD fraternity and Biorobtics lab with a special mention to Ashwin George for offering his bizarre yet interesting perspectives on my research problems during our conversations in the library, Aneesh Ashok Kumar for his valuable feedback on the manuscript of this report, and Simon van der Helm for helpful suggestions during our meetings.

A special thanks to my closest friends Ir.Getssy Prathiba, Ir.Ragavendar Thrivikram Ganesh, Padmapriya Arulkumar, and Ir.Avin Shanbhag who made the journey through my masters studies at TU Delft pleasurable and enjoyable.

Above all, I would like to thank my wonderful parents and sister for always being there for me through my life and studies. Finally, I would like to thank the Almighty for everything that I am blessed with. எல்லா புகழும் இறைவனுக்கே (All praise to the lord).

*Rahul Ramesh*

*Delft, November 2019*

# Abstract

The Sit-to-Stand (SiSt) task is one of the most crucial yet mechanically demanding daily tasks. A transfemoral amputee develops high torques on the intact leg to complete the SiSt task. Such high torques are a consequence of limited torques produced by a prosthesis. The main interest of this project is on the sit-to-stand task of a transfemoral amputee fitted with an active knee and passive ankle prosthesis. The objective is to test whether strategies like asymmetric foot placement and reduced weight-bearing asymmetry could reduce the torque produced in the intact knee. Musculoskeletal model of an able-bodied human subject and a transfemoral amputee subject enabled with an active knee prosthesis is developed. Forward dynamic optimisations are performed by defining an appropriate framework required for simulating the sit-to-stand task. The process was verified by implementing the framework on the musculoskeletal model of an able-bodied individual and comparing it with experimental results available in the literature. The comparison showed a good agreement of simulated results with results reported in the literature. Joint torque profiles of the intact limb of the amputee model were then simulated with asymmetric foot placement and reduced weight-bearing asymmetry strategies. Placing the prosthetic leg posterior to the intact leg reduced the peak intact knee torques by 1.5% relative to placing the intact leg adjacent to the prosthetic leg. The peak intact knee joint torques were reduced by 13% in SiSt task simulation with reduced weight-bearing asymmetry. An increased metabolic cost needed to perform the SiSt task also resulted from this strategy.

This report is towards the completion of the course, **ME51032 - ME-BMD MSc Project**
R. Ramesh (4750284), Delft, The Netherlands

# Effect of Asymmetric Foot Placement and Reduced Weight-Bearing Asymmetry on the Sit-to-Stand Task of a Unilateral Transfemoral Amputee – A Simulation Study

Rahul Ramesh

***Abstract*—The Sit-to-Stand (SiSt) task is one of the most crucial yet mechanically demanding daily tasks. A transfemoral amputee develops high torques on the intact leg to complete the SiSt task. Such high torques are a consequence of limited torques produced by a prosthesis. The main interest of this project is on the sit-to-stand task of a transfemoral amputee fitted with an active knee and passive ankle prosthesis. The objective is to test whether strategies like asymmetric foot placement and reduced weight-bearing asymmetry could reduce the torque produced in the intact knee. Musculoskeletal model of an able-bodied human subject and a transfemoral amputee subject enabled with an active knee prosthesis is developed. Forward dynamic optimisations are performed by defining an appropriate framework required for simulating the sit-to-stand task. The process was verified by implementing the framework on the musculoskeletal model of an able-bodied individual and comparing it with experimental results available in the literature. The comparison showed a good agreement of simulated results with results reported in the literature. Joint torque profiles of the intact limb of the amputee model were then simulated with asymmetric foot placement and reduced weight-bearing asymmetry strategies. Placing the prosthetic leg posterior to the intact leg reduced the peak intact knee torques by 1.5% relative to placing the intact leg adjacent to the prosthetic leg. The peak intact knee joint torques were reduced by 13% in SiSt task simulation with reduced weight-bearing asymmetry. An increased metabolic cost needed to perform the SiSt task also resulted from this strategy.**

## I. Introduction

The Sit-to-Stand (SiSt) transition is a repeatedly performed task and a crucial pre-requisite for other daily activities [1]. It also requires a high mechanical demand [2]. The task proves to be harder in unilateral transfemoral amputees who lack the crucial knee and ankle joint to perform the SiSt task [3]. Assistive devices, such as lower limb prosthesis, help amputees regain this basic functional ability. However, such devices might not possess the required strength to drive the body from a sitting posture to a standing posture.

Prosthetic devices have limited torque producing capabilities. Performing the SiSt task despite such a limitation causes the intact knee to produce higher than normative torques. Repeated attempts to perform this task leads to secondary health conditions such as osteoarthritis and osteoporosis [4]. Therefore, it is of importance to reduce the effort put by the intact knee.

One solution to the identified problem could be a support torque from the prosthesis adjusted to the task and the physical abilities of the user. However, current prosthetic devices mostly only dissipate energy. Therefore, they cannot take off the load from the sound leg in a task that requires positive power, like sit-to-stand. Furthermore, powered prostheses mostly produce only limited output torque, because of weight considerations. Thus, a secondary solution is required in conjunction with an active support torque from the prosthesis. This work aims at testing two such solution strategies.

Various strategies for performing the SiSt task have been cited in the literature [5][1]. Burger et al., (2005) stated that a unilateral transfemoral amputee accounts for the missing limb by employing such alternative strategies [3]. Burger and colleagues tested this and reported a modulation in the position of the feet before starting the task as a possible alternative strategy.

The literature presents evidence of foot placement affecting the SiSt transition [3], [5]–[7]. Elderly and disabled individuals prioritise stability over lower joint loads. Thus, such group of people position themselves in the most stable orientation while sitting before transitioning to a standing posture [7]. The SiSt task performance is more stable if the distance between the Base Of Support (BOS) and the Centre Of Mass (COM) is small before the task begins. The BOS is the area enclosed by the feet during the rising motion. The condition for the most stable sitting configuration before starting to rise can be achieved by positioning the feet posterior to a neutral position before rising to the standing posture. This behaviour is observed in the case of Hughes et al., (1994) [7] who reported that older subjects moved their feet posterior to the neutral position (ankle joint is aligned with the knee) in order to reduce the distance between the COM and the feet (BOS).

Such a foot placement strategy is shown to affect the lower limb joint torques substantially [6]. Reduction of the distance between the COM and the BOS before beginning to ascend to the standing posture reduces the distance and the duration needed for the generation of sufficient horizontal momentum and thus implying a greater contribution of torque generated by the lower limb joints. A number of studies including Gillette et al., (2012) [6], Mathiyakom et al., (2005) [8], Fleckenstein et al., (1998) [9] and Kawagoe et al., (2000) [10] supports this fact.

Gillette and colleagues [6] also studied the effect of asymmetric foot placement on the sit-to-stand task in healthy subjects [6]. It was observed that higher loads occur in the limb placed closer to the body than away from the body. A study investigating the effect of foot placement on the sit-to-stand

The author is with the Delft University of Technology R.Ramesh-1@student.tudelft.nl

[1]Refer Appendix A for an elaborate description of the nominal SiSt task, which is widely performed by healthy able-bodied subjects

task in patients with hemiplegia reported an increase of 39% in the EMG levels of the healthy limb when the hemiplegic limb (un-involved limb) was placed in lower knee flexion (anterior to the healthy limb) [11].

There are reports in the literature of transfemoral amputees with passive and active prosthetic legs, performing the SiSt task with symmetric foot placement [3], [12], [13]. These studies, however, were only interested in the degree to which the kinetic and kinematic parameters are asymmetric due to transfemoral amputation. The literature lacks studies examining the effect of asymmetric foot placements on individuals with active knee prosthesis.

Based on the results of the surveyed literature regarding foot placement strategies, it was speculated that asymmetric foot placement could result in a more normal load distribution between the limbs. It has also been established in the literature that for an able-bodied individual, anteriorly placed limb bears less effort than the posterior limb. It is therefore hypothesised that this strategy could be used to redistribute the knee torques from the intact limb to the prosthetic limb. In this case, the prosthetic leg will be placed posterior to the neutral position while the intact leg is placed anterior to the neutral position.

A major drawback of using transfemoral prosthesis as an aid for standing up is increased weight-bearing asymmetry between the two limbs [3], [14]. Able-bodied subject show minute asymmetries in the joint torques and angles while performing the SiSt task [3], [15], [16]. On the other hand, transfemoral amputees exhibit a greater magnitude of asymmetry. Simon et al., (2016) attributes this behaviour to a lack of complete torque support from the prosthesis [14]. As a consequence, the amputee is forced to use more of the intact limb thereby increasing the level of asymmetry. Another reason for the a greater magnitude of asymmetry could also be due to a lack of proprioception from the prosthetic device. Proprioception feedback is an essential component in maintaining balance. A lack of this essential component reduces the trust of the amputee on the prosthetic device and increases the use of the intact limb in performing the SiSt task.

Simon et al., (2006) demonstrated that by using a powered knee-ankle prosthesis, the weight-bearing asymmetry could be reduced [14]. However, it is still substantially higher than for a healthy able-bodied subject who tend to load their limb almost symmetrically. The literature is still to examine the effect of a transfemoral amputee with an active knee prosthesis intentionally loading the prosthetic limb on the kinetics of the intact limb. This scenario is also tested in this work.

An analysis to test such solution strategies can be approached from two fronts. The first is by analysing high volumes of motion capture and force plate data derived from experimentation to simulate the joint torques. Although this method shows prominence in the field of locomotion studies, it is not always reliable and safe. High variability and subjectivity of individuals performing these experiments may sometimes lead to inconclusive results. A viable alternative is physics-based forward dynamic simulations which are independent of motion capture data [17]. Such simulations predict the motion of any biological organism, given a set of mathematically defined rules describing the motion; and a musculoskeletal model that represents the organism in question. It tries to map the workings of the Central Nervous System (CNS) in determining an optimal set of excitation signals which gets transformed to control signals to drive muscles of the musculoskeletal model to bring about the desired motion. Figure 1 pictorially depicts a simplified framework of such a simulation technique.

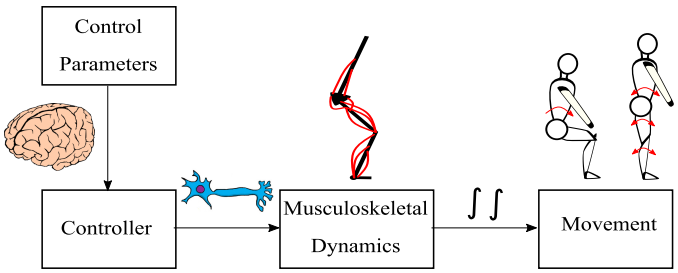


Fig. 1. Representation of a simplified forward dynamic simulation framework[2].

The goal of this work is to use predictive forward dynamic simulation to test the effect of strategies like asymmetric foot placement and reduced weight-bearing asymmetry on the torques produced in the intact knee of a transfemoral amputee. The transfemoral amputee model is enabled with an active knee and passive ankle prosthesis.

This work uses OpenSim, a freely available software used for modelling musculoskeletal systems and perform dynamic simulations on said models [18]. The predictive simulation framework is built in an open-source software called SCONE, a dedicated software for predictive simulation of biological motions [19].

## II. Methodology

### A. Modelling of the musculoskeletal system

The entire musculoskeletal model is based on a planar 10 Degrees Of Freedom (DOF) lower limb model with a rigid trunk segment developed in OpenSim (Authored by Ajay Seth, Darryl Thelen, Frank C. Anderson and Scott L. Delp). This model is adapted and converted to a 9-DOF model in SCONE (by Thomas Geijtenbeek). The trunk segment from the original model was modified to represent a realistic trunk. The parameters of such a trunk segment were derived from [20]. This segment is further attached with neck, and head segments derived [21].

The modified musculoskeletal model is a structure consisting of 22 segments, 20 joints and 14 degrees of freedom. It consists of a total of 20 muscles which includes 16 lower limb muscles and 4 upper limb muscles. These muscles are capable of producing actuation only in the sagittal plane and are modelled as equilibrium muscle models, as described in Millard et al. (2013), [22], to bring about the prescribed joint actuation.

Representation of major segments, joints and muscles are shown in Figure 2. Appendix B and C elaborates more on the

[1]The brain and neuron clipart is taken from http://clipart-library.com and https://www.brainfacts.org respectively

topology of the musculoskeletal model, equilibrium muscle models, motivation behind the selection of specific muscle properties and ligament properties along with the derivation of the parameters of the seat-buttocks contact model.

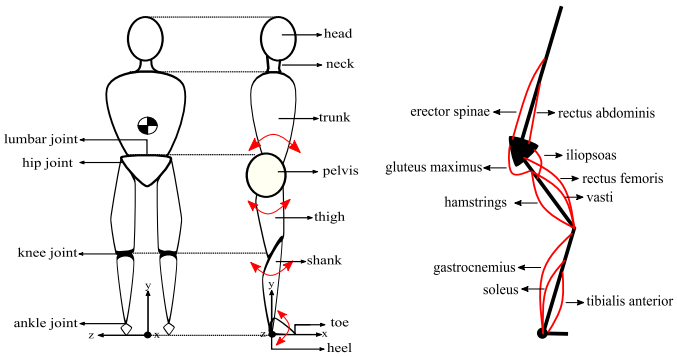


Fig. 2. Segments and muscles included in the musculoskeletal model. Muscles present in one side of the sagittal plane is depicted here. Similar muscles are present on other side of the plane.

The 9-DOF model in SCONE did not include the trunk muscles and relied only on the iliopsoas muscle to actuate the trunk. Since the SiSt task simulation requires a significant amount of trunk flexion in the sagittal plane, rectus abdominis and erector spinae muscles were chosen to be included [23]. Furthermore, the muscle strengths also had to be modified to capacitate the muscles to bring about the required joint torques.

Ligaments were necessary for the model to maintain the prescribed joint ranges of motion (values of which are referred from AAOS standards [24]). Ligaments were modelled as passive spring-damper elements in our musculoskeletal model. These are implemented using the 'CoordinateLimitForce' functionality in OpenSim. These ligaments were incorporated at the knee, hip and trunk joints of the musculoskeletal system. These three locations were mainly chosen because the largest flexion and extension are observed at these joints during the SiSt task and thus should be kept within limits to prevent any infeasible solutions during simulations.

The model is incorporated with contact models at five locations in the musculoskeletal system. The segment in contact with an environment is represented as spheres, and the environment itself was modelled as complaint half-spheres, which deform as a result of the contact spheres pressing against it during the motion. Figure 3 illustrates this behaviour. This interaction between the spheres and half-spheres depend upon the net normal force and the force of friction. Properly parameterised normal forces and frictional forces combine to ensure unilaterality and realistic slip between the two interacting surfaces. Four of the five contact models were placed in the toe and heel of each foot, and the fifth sphere representing the buttocks was placed in the rear of the pelvis. The development of the normal force ($F_{\mathrm{N}}$) between the foot and the ground is based on the Hunt-Crossley model [25], characterised by Equation 1. The geometries (radius of the contact sphere and location with respect to the heel and toe) and the parameters for modelling the foot-ground contact model were adapted directly from Gilchrist et al., (1996) [26] and implemented in the model.

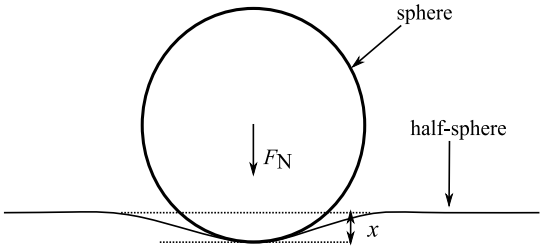


Fig. 3. Illustration of the interaction between sphere and half-sphere, used for deriving the contact force, ($F_{\mathrm{N}}$).

$$F_{\mathrm{N}} = kx^{\frac{3}{2}}(1 + \frac{3}{2}c\dot{x}) \tag{1}$$

Where $F_{\mathrm{N}}$ is normal force component, $x$ is the depth of penetration of the contact sphere into the contact half-sphere and $\dot{x}$ is the rate of the depth of penetration of the contact sphere into the contact half-sphere.

The normal force ($F_{\mathrm{N}}$) between the seat and the buttocks is based on the Elastic Foundation Theory [27], characterised by Equation 2. The geometry (radius of the contact sphere and location with respect to the pelvis) for this model is based on the studies by Linder-ganz et al., (2007) [28]. Appendix C delineates the reason for the selection of the Elastic Foundation Force to characterise the seat-buttocks contact model and the method for deriving its parameters.

$$F_{\mathrm{N}} = kx(1 + \frac{3}{2}c\dot{x}) \tag{2}$$

The elements of the Equation 2 have the same meaning as the elements of Equation 1.

Both types of contact models share the same friction equations to characterise the friction force ($F_{\mathrm{F}}$) at the contact locations. Equation 3 represents the friction model.

$$F_{\mathrm{F}} = F_{\mathrm{N}}(u_{\mathrm{d}} + 2(u_{\mathrm{s}} - u_{\mathrm{d}})) + u_{\mathrm{v}}v_{\mathrm{s}} \tag{3}$$

Friction force component is represented as $F_{\mathrm{F}}$, $u_{\mathrm{s}}$ is the coefficient of static friction, $u_{\mathrm{v}}$ is the coefficient of viscous friction and $u_{\mathrm{d}}$ is the coefficient of dynamic friction and $v_{\mathrm{s}}$ is the slip (tangential) velocity of the two bodies at the contact point. Table I lists the parameters of the contact models.

The existing model was tweaked to represent a transfemoral amputee. The left leg was chosen to represent the prosthetic leg. This choice did not affect the approach to the solution in any sense. An active knee prosthesis with a passive ankle is considered in this work. It is assumed that about half of the femur is lost as a result of the amputation. Tibialis anterior, soleus, gastrocnemius and the vasti muscles are removed from the left leg of the model. The biarticular hamstrings and rectus femoris muscles are attached to the point where the femur is assumed to be amputated. Upon the modifications to the assumed amputated leg, the moment delivering capacity of the hip reduced. Figure 4 depicts this attribute, which plots the hip torque as a function of hip angle before and after amputation.

TABLE I
PARAMETER VALUES OF THE CONTACT MODELS

| Model | Stiffness, $k$ (in Nm) | Dissipation, $c$ (in Ns/m) | Static friction coefficient $u_s$ | Dynamic friction coefficient $u_d$ | Viscous friction coefficient $u_v$ |
|---|---|---|---|---|---|
| foot-ground model | 2.00E+06 | 1.0 | 0.9 | 0.8 | 0.6 |
| seat-buttocks model | 147450 | 5110 | 0.9 | 0.8 | 0.6 |

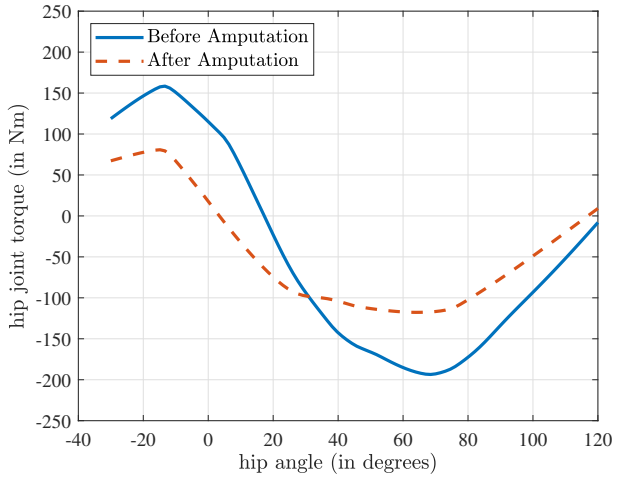


Fig. 4. Plot depicting the reduction of hip extension torque after amputation.

TABLE II
PROPERTIES OF THE TRANSFEMORAL PROSTHESIS MODEL

| Prosthetic Joint | Actuation type | Maximum Torque Capacity (in Nm) | Stiffness (in N/m) | Damping Coefficient (in Ns/m) |
|---|---|---|---|---|
| **Knee** | active | 30 | - | - |
| **Ankle** | passive | - | 10 | 0.25 |

It should be noted that this study excludes the effect of socket types and length of residual limbs from the scope of this study.

The mass of the prosthesis is reduced to weigh 1.5 times less than a natural leg, and the inertia properties were scaled from the inertial properties of a natural leg to match the properties of the new mass of the leg.

The knee is provided with a maximum capacity of 30 Nm (0.3896 Nm/kg) which is 5 Nm more than a value deemed suitable by Varol et al., (2009) [29] to perform the SiSt task with an active prosthetic leg. The passive properties of the ankle match that of a natural ankle and the parameters representing this passive force is referred from Weiss et al., (1986) [30]. Table II provides the properties of the active knee actuator and the passive ankle.

### *B. Simulation of the sit-to-stand task*

A predictive motion simulation framework is built for the simulation of the SiSt task. The framework consists of a model, a controller, and an objective function. Each of these components is elaborated as follows.

An essential component for forward dynamic simulations is an adequate musculoskeletal model. The musculoskeletal model should consists of properly defined skeletal structure incorporated with biological constraints (joint ranges of motion), contact models and most importantly, controllable actuators such as muscular-tendons or torque actuators. The complexity of the model depends upon the comprehensiveness of the intended analysis. The SiSt motion required an extensive definition of the musculoskeletal model as elaborated in the previous section and Appendix B.

The model is actuated by a set of control signals fed into the actuators (muscles in case of natural limbs and torque actuators in case of prosthetic limbs) by the controller. An objective function needs to be defined which is either maximised or minimised during the optimisation. The objective function describes the characteristics of the motion being simulated.

The objective function returns a numerical value which is either minimised (in case of an error measure) or maximised (in case of a performance measure) based on the motion in question. The optimisation process proceeds as the optimiser (an optimisation algorithm) varies the control and model parameters in search of an appropriate set of parameter values which either minimises or maximises the objective function. The final set of optimised parameters brings about the intended motion. SCONE allows the optimisation of both control parameters and model parameters. The current application does not optimise the model parameters rather optimises only the control parameters. The optimiser uses 'Covariance Matrix Adaptation Evolution Strategy (CMAES)' algorithm to compute the optimal parameters [31]. Appendix D delineates the principle of this algorithm.

The following subsections elaborate more on the control model and its parameters, followed by a description of the objective function used for simulating the SiSt task.

*1) Controller:* A parametric feedforward control model is defined for controlling the temporal muscle excitation values, $e$. These muscle excitations get translated to muscle activation, $a$, through a first-order activation dynamics (refer Equation 16 in Appendix B). Based on the value of muscle activation, a muscle force is generated, which gets multiplied to a moment arm value to generate the torque about a joint. Figure 5 depicts the feedforward control leading to the output musculoskeletal force.

A piecewise-linear function is chosen to represent the excitation signal. 10 equally spaced control nodes, with a fixed time interval of 0.12 s, are chosen to control the excitation pattern ($t_{\text{sim}}$ is the total simulation time in seconds). The choice

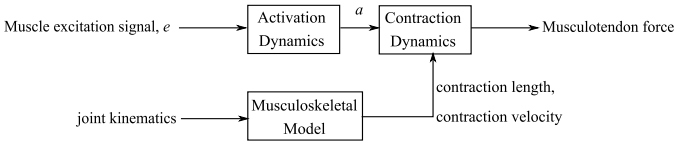


Fig. 5. Flow diagram describing the process of producing a musculotendon force starting from a muscle excitation signal (diagram adapted from [22]).

of the number of control nodes involves a trade-off between the computational effort and sensitivity of the simulation to changes in the number of control nodes. Ten control points satisfied this trade-off. The optimiser aims to vary the values of these ten fixed-interval control nodes to simulate the SiSt task optimally. These control nodes form the optimisation parameters. Each muscle in the musculoskeletal model consists of these ten parameters (values of the control nodes) which indirectly determine their action.

For simulations that did not involve a prosthetic limb, bilateral symmetry was assumed. In such a case, the feedforward controller provides similar excitations to similar muscle groups on either half of the body (this is referred to as the 'symmetric property' in subsequent sections). Therefore, for such a case, only half the parameters were optimised.

*2) Optimised sit-to-stand motion:* The parameters of the feedforward controller function described in the previous section are determined through an evolution-based optimisation strategy called Covariance Matrix Adaptation Evolution Strategy (CMAES), as described in Hansen, (2006) [31]. The CMAES algorithm used in this work used a step size 0.005, and a 15 member sized population at each iteration. Each member of the generated population is used for evaluating the objective function to test its strength. Appendix D provides more information on the CMAES algorithm.

The optimisation of a SiSt transition for a healthy able-bodied model consists of a total of 20 muscles to be controlled. The symmetric property is enabled for this case which reduced the number of muscles to control to 10. Each muscle has ten parameters, thus bringing the total number of parameters to be optimised to 100.

For the prosthesis model, the number of muscles gets reduced to 16, and an additional torque actuator is added. In this case, the symmetric property cannot be enabled.

The optimiser aims to minimise the function $\mathcal{O}$.

$$\mathcal{O} = E_{\text{SiSt}} + P_{\text{SiSt}} \tag{4}$$

Where $\mathcal{O}$ is the penalised objective function, $E_{\text{SiSt}}$ is the unpenalised objective function and $P_{\text{SiSt}}$ is the penalty function.

Each of the two functions on the right-hand side of Equation 4 is elaborated as follows.

$$\begin{aligned} E_{\text{SiSt}} = E_{\text{COMpos}} + E_{\text{config}} + E_{\text{COMvel}} + E_{\text{lift}}(t) + \\ E_{\text{slip}}(t) + E_{\text{effort}}(t)) \end{aligned} \tag{5}$$

The unpenalised objective function consists of five weighted terms, and each term fulfils a specific purpose in simulating the SiSt motion. The first three terms of the objective function are time-independent and are evaluated only in the last time frame. The last three terms, however, are time-dependent and are obtained by integrating over the entire simulation time ($t_{\text{sim}}$).

An important condition for performing the SiSt task is that the foot does not rise from the ground or slip relative to the ground. This criterion is modelled using two-time dependent terms $E_{\text{rise}}(t)$ and $E_{\text{slip}}(t)$ respectively. The following equations represent these two terms.

$$E_{\text{lift}}(t) = \int_0^{t_{\text{sim}}} y_{\text{toe}}(t)\,\mathrm{d}t \; + \; \int_0^{t_{\text{sim}}} y_{\text{heel}}(t)\,\mathrm{d}t \tag{6}$$

$$E_{\text{slip}}(t) = \int_0^{t_{\text{sim}}} (x_{\text{toe}}(t) \; - \; x_{\text{toe}}(0))^2\,\mathrm{d}t \tag{7}$$

Where, $y_{\text{toe}}$ and $y_{\text{heel}}$ are the vertical centre of mass displacements of the toe and heel bodies respectively and $x_{\text{toe}}$ is the horizontal COM displacement of the toe. The term $E_{\text{lift}}$ aims to minimise the integral of the vertical displacement of the toe and the heel over time. The square of the difference between the horizontal displacement of the toe and the initial position of the toe is minimised to prevent foot slippage. Since there is no horizontal displacement of the toe and heel relative to each other, only the toe body is considered in the $E_{\text{slip}}$ term.

The SiSt task ends with quiet-standing. Two essential conditions should be satisfied to achieve quiet-standing. The first condition requires the COM to settle inside the base of support and the second condition requires the centre of mass velocity to be close to zero. The first condition is tackled by term $E_{\text{COMpos}}$. This term ensures that the centre of mass of the model lies within the BOS, which is bound by the two extremities of the foot (toe and the heel). The term is mathematically represented as follows.

$$E_{\text{COMpos}} = (x_{\text{COM}} - x_{\text{BOS}})^2 \tag{8}$$

In the above equation, $x_{\text{BOS}}$ and $x_{\text{COM}}$ corresponds to the horizontal displacement of the centre of mass and base of support respectively. The BOS, in the case of asymmetric foot placement, is bounded by the heel of the anteriorly placed leg and the toe of the posteriorly placed leg. In the case of symmetric foot placement, the BOS is bound by the heel and toe of either leg.

The second condition required for quiet-standing is satisfied by the $E_{\text{COMvel}}$ term. It ensures that the model comes to a halt at the end of the motion by minimising the sum of the square of the horizontal ($v_x$) and vertical ($v_y$) centre of mass velocities. The value of this term is computed in the last time frame and added to the objective function.

$$E_{\text{COMvel}} = v_x^2 \; + \; v_y^2 \tag{9}$$

To ensure that a proper configuration is reached at the end of the motion simulation, the term $E_{\text{config}}$ is used. This term penalises any deviation from the target configuration. For a proper standing configuration, the relative angles of the knee, pelvis and trunk angles should be close to zero. Figure 5 illustrates the joint angle definitions. Thus, the $E_{\text{config}}$ term

minimises the squares of the knee, pelvis and trunk angles. It is mathematically modelled as follows.

$$E_{\text{config}} = \theta_{\text{knee}}^2 + \theta_{\text{pelvis}}^2 + \theta_{\text{trunk}}^2 \tag{10}$$

Lastly, the effort needed to perform the SiSt task is minimised by defining an effort term, $E_{\text{effort}}(t)$, which outputs the rate of metabolic energy consumed during the task. The method of computing the effort term is delineated in [17]. Appendix F elaborates on the $E_{\text{effort}}$ term.

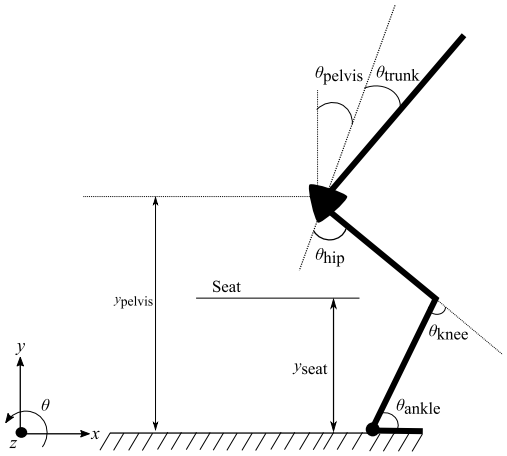


Fig. 6. Definition of the joint and seat coordinates used in this study.

Each term in the objective function is weighted to scale the terms relative to each other. These weights differed depending upon the type of simulation experiment being performed. It should be noted that the weights for the time-dependent terms are multiplied to the final integrated values.

A penalty term was added to the unpenalised objective function to restrict the solution search space. This penalty function is dependent on how good the simulation is performing; i.e., if a specific undesired condition is encountered early-on in the simulation, a high penalty is added to the unpenalised objective function. The penalty reduces as the time of encountering the undesired condition increases. A lower penalty is added to the unpenalised objective function as the time at which these termination conditions are met close to the maximum limit on the simulation duration. These are mathematically represented in equations 12 and 13. Such a means of including the penalties, drive the simulation towards a better and feasible solution.

The study by Geijtenbeek et al., (2013) incorporated termination conditions in their simulation studies [32]. This ensured that local minima were not reached and drove the simulation towards the desired solution. Adding terminal conditions to the simulation also saved computational cost. Such a strategy was also implemented in this simulation by terminating the simulation when the undesired condition is leading to the application of a penalty. These conditions are checked at each time frame, and if a specific condition is satisfied, the simulation is immediately stopped and highly penalised. The overall penalty function is expressed as follows.

$$P_{\text{SiSt}} = P_{\text{fast}} + P_{\text{fall}} \tag{11}$$

$P_{\text{SiSt}}$ measures the absolute value of the horizontal centre of mass velocity ($v_x$) at every time frame to check for falling. If it increases beyond a certain threshold, the simulation is terminated, and the following penalty is applied.

$$P_{\text{fall}} = \begin{cases} c \cdot \frac{t_{\text{max}}}{t_{\text{sim}}} & |v_x| > 0.1\text{m/s} \\ 0 & \text{otherwise} \end{cases} \tag{12}$$

$P_{\text{fast}}$ measures the value of the vertical centre of mass velocity ($v_y$) at every time frame to check for a fast-rising movement. If it increases beyond a certain threshold, the simulation is terminated, and the following penalty is applied.

$$P_{\text{fast}} = \begin{cases} c \cdot \frac{t_{\text{max}}}{t_{\text{sim}}} & v_y > 1\text{m/s} \\ 0 & \text{otherwise} \end{cases} \tag{13}$$

The factor of $c$ in equations 12 and 13 is for scaling the penalties to a higher proportion than the other measures in the unpenalised objective function. Doing so is an indicator to the optimiser to prioritise the minimisation of the penalties over the unpenalised objective function.

There exists an additional "passive" termination condition, which does not influence the objective function. This condition checks if the standing posture has been reached. The condition for stand posture is a particular combination of joint angles and centre of mass height which is checked at each time instant, and if the condition is satisfied, the simulation is stopped.

Simulations of the SiSt transition involving a model of healthy able-bodied individual and an individual with a unilateral transfemoral prosthesis were performed using the above optimisation framework.

Specific modifications was made to the objective function to test the condition of reduced weight-bearing asymmetry on the SiSt task simulation using a unilateral transfemoral amputee model.

An additional term, named as '$E_{\text{SymGRF}}$', was included in the unpenalised objective function to force the prosthetic knee to utilise a higher proportion of its maximum possible output. This term ensures that an SiSt task strategy with reduced asymmetry in the loading of the two legs is reduced (ground reaction force is used as a measure to realise the loading between the two legs). This objective function term is represented mathematically in Equation 14.

$$E_{\text{SymGRF}} = \int_0^{t_{\text{sim}}} (GRF_{\text{L}} - GRF_{\text{R}})^2 \, \mathrm{d}t \tag{14}$$

Where $GRF_{\text{L}}$ is the ground reaction force component of the left foot and $GRF_{\text{R}}$ is the ground reaction force component of the right foot.

In order to quantitatively compare results across all the simulation conditions, a measure defined by Highsmith et al., (2011) [13], called the Degree of Asymmetry (DoA) was used to compute the difference in the ground reaction forces. The DoA is mathematically defined as

$$DoA = \frac{\text{Intact side - Prosthesis side}}{\text{Intact side + Prosthesis side}} \cdot 100. \tag{15}$$

## III. Simulation Experiments & Results

### *A. SiSt task simulation of a healthy able-bodied model with symmetrical foot placement*

The objective of this experiment was to test the framework described in the previous section on a musculoskeletal model of a healthy young able-bodied individual. The model was positioned using the initial conditions mentioned in Table III. The joint definitions were as per AAOS standards [24] and are depicted in Figure 6. It should be noted that this experiment was performed with a symmetrical foot placement strategy. The initial conditions were set such that the model starts from a position where the COM is close to the BOS. An elderly or disabled individual would start the SiSt movement [3], [7] from this configuration. This initial condition was chosen because a uniformity could be maintained for easier and consistent comparison of results within the experiments. The seat was placed at 100% knee height in accordance with the study by [33]. Arm support or back support were not incorporated into the model.

The muscle excitation parameters were initialised at 30% of their maximum capacities, and the maximum limit on the simulation duration ($t_{\max}$) was set to 1.2 s. 10 control points separated by 0.12 s parameterised the excitation signals. Once the optimisation scenario was set, it was evaluated once to test if all the objective function terms are rightly initialised. The optimisation was initiated once all the initialisation were verified.

Figure 7, 8, 9 and 10 show the results of the experiment involving the healthy able-bodied musculoskeletal model. Hip and knee joint kinematics and kinetics are chosen as appropriate measures for comparison. Both the measures are plotted as a function of time as a percentage of movement duration.

The study by Doorenbosch et al., (1994) [34], Pai et al., (1991) [35], and Bajelan et al., (2014) [36] are chosen for comparison of joint kinematics; and the study by Hutchinson et al., (1994) [37] along with joint moment data by Doorenbosch et al., (1994) and Pai et al., (1991) is used for comparing joint kinetics. For a normative means of comparison, the data were normalised with the body weight and presented here.

The feet were placed symmetrically, and the simulation was started from an initial condition indicted in Table IV. The simulation took 0.790s to complete.

Knee joint kinematics show a good agreement with the reported knee joint angle data in the literature. However, the results from the literature show a greater hip flexion initially as compared to the hip angles resulting from the simulation.

The hip and knee torque values resulting from this simulation experiment peaked at greater values than the values reported by Doorenboch et al., (1994), Pai et al.,(1991) and Hutchinson et al., (1994) [34], [35], [37]. Simulation of the SiSt task performed with a model of the able-bodied individual produced a peak knee and hip torque of 1.38 Nm/kg and 1.17 Nm/kg respectively as compared to 0.81 Nm/kg and 0.59 Nm/kg in Doorenbocsh et al.,(1994), 1.11 Nm/kg and 0.5945 Nm/kg in Pai et al., (1991) and 1.23 Nm/kg and 0.51 Nm/kg in Hutchinson et al., (1994). It is evident from the plots that there is considerable variation amongst the results

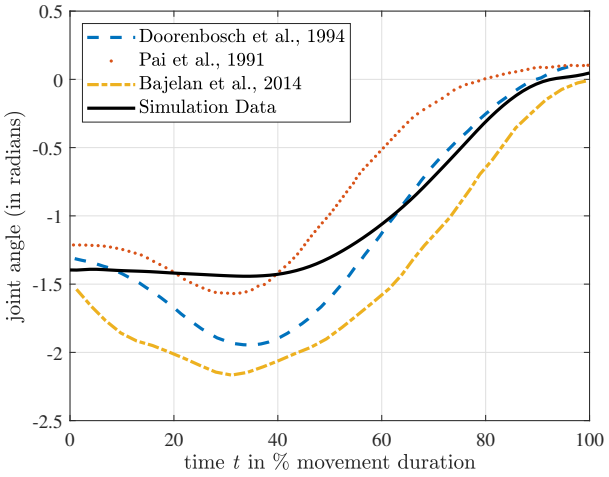


Fig. 7. Hip joint angle trajectory of the simulated SiSt task compared with hip joint angle trajectory reported in literature (Data derived from [34], [36] and [35]).

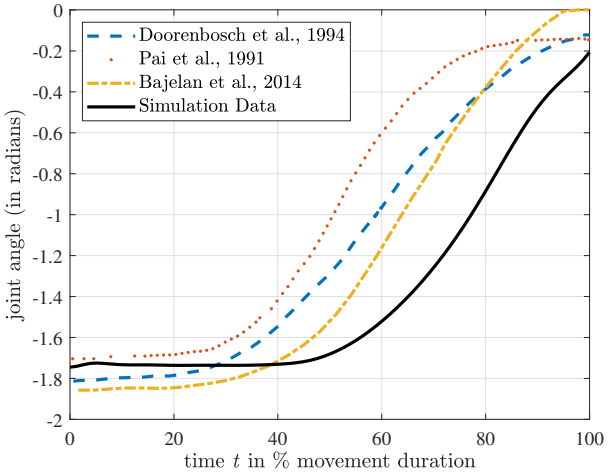


Fig. 8. Knee joint angle trajectory of the simulated SiSt task compared with knee joint angle trajectory reported in literature (Data derived from [34], [36] and [35]).

in the literature. Nevertheless, the plot shows an agreement in the trend of these joint kinetic data. Joint torques also peak at different instances during the SiSt motion, nonetheless, are in the vicinity of each other.

Simulation time is considerably different from the movement times reported in the studies for moving from a seated position to standing position. Figure 11 summarises these differences in task performance time and simulation time.

### *B. SiSt task simulation of a unilateral transfemoral amputee model with active knee prosthesis to test the effect of foot placement*

This experiment was intended to observe the performance of the transfemoral amputee model in performing the SiSt motion with different foot placement strategies and to observe the trend in the hip and knee joint torques.

TABLE III
INITIAL CONDITION FOR SYMMETRIC FOOT-PLACEMENT STRATEGY SIMULATIONS

| **Coordinate** | $y_{\text{pelvis}}$ **(in m)** | $\theta_{\text{pelvis}}$ **(in rad)** | $\theta_{\text{trunk}}$ **(in rad)** | $\theta_{\text{hip}}$ **(in rad)** | $\theta_{\text{knee}}$ **(in rad)** | $\theta_{\text{ankle}}$ **(in rad)** | $y_{\text{seat}}$ **(in m)** |
|---|---|---|---|---|---|---|---|
| **Magnitude** | 0.638 | -0.227 | -0.546 | 1.39626 | -1.74533 | 0.576 | 0.500 |

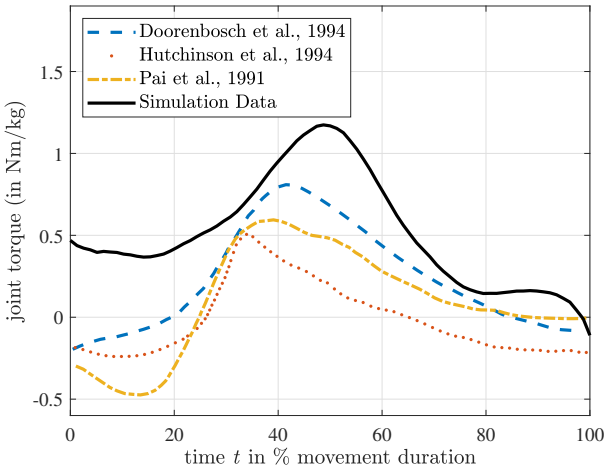


Fig. 9. Hip joint torque trajectory of the simulated SiSt task compared with hip joint angle torque reported in literature (Data derived from [34], [37] and [35]).

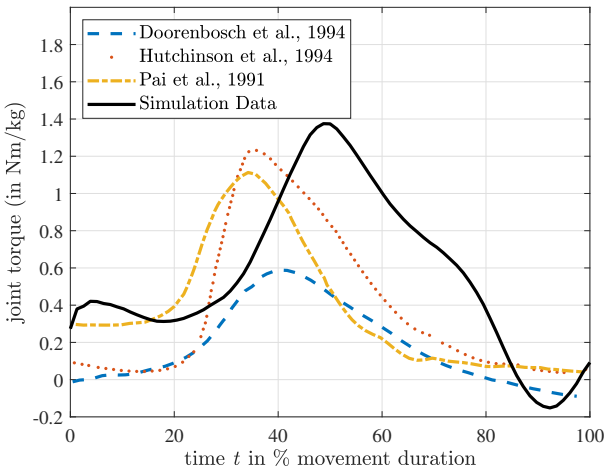


Fig. 10. Knee joint torque trajectory of the simulated SiSt task compared with knee joint angle torque reported in literature (Data derived from [34], [37] and [35]).

Three cases of foot placements were simulated. The first case (Case 1) was with an asymmetric foot placement strategy where the intact leg is trailing the prosthetic leg (Intact leg behind prosthetic leg). This case follows the initial condition described in Table IV. The second case (Case 2) was a symmetric foot placement strategy (Both legs are adjacent to each other) following the initial conditions mentioned in Table III. The third case (Case 3) was an asymmetric foot placement with the prosthetic leg trailing the intact leg (prosthetic leg

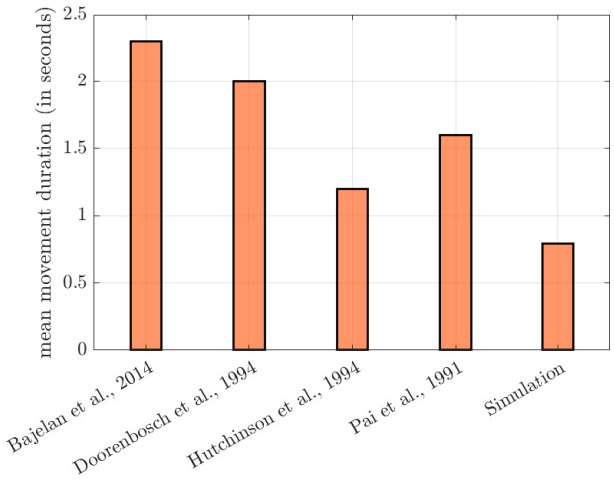


Fig. 11. Comparison of the movement time of the simulated SiSt task with the movement time reported in literature (Data derived from [34], [36], [37] and [35]).

behind intact leg) following the initial conditions tabulated in Table IV. The results of the asymmetric foot placement strategies (case 1 & case 3) are compared to the symmetric foot placement strategy (case 2).

The simulation scenario was similar to the earlier experiment with the able-bodied musculoskeletal model. Similar seat height and maximum duration were used. The muscle excitation was parameterised with 10 control points separated by 0.12 s and initialised at 30% of their maximum capacities. The objective function was evaluated to test if all the objective function terms were rightly initialised. The optimisation was initiated once the initialisation was verified.

Figure 12 shows the effect of different foot placement strategies on the peak intact knee torque. A trend emerges from the plot which showcases an increase in peak knee torques as the healthy foot moves from the leading position to the trailing position. Consequently, a decrease in peak knee torque in the prosthesis is also noted (refer Figure 13). Table V tabulates the DoA associated with different foot placement strategies.

A peak of $1.98\,\mathrm{Nm/kg}$ is delivered by the intact knee and a peak of $0.37\,\mathrm{Nm/kg}$ is delivered by the prosthetic knee in case 3. This result is a reduction of 1.55% in the torque of the intact knee and an increase of 11.84% in the peak knee torques of the prosthetic knee from case 2. Case 3 caused a 68% and 37% of asymmetry in knee and hip torques between the two limbs.

The intact knee torques peak at $2.19\,\mathrm{Nm/kg}$ following a peak of $0.29\,\mathrm{Nm/kg}$ delivered by the prosthetic knee in the case 1. This is an increase of 7.3% in the torque of the intact knee and a decrease of almost 17% in the knee moments of

TABLE IV

INITIAL CONDITION FOR ASYMMETRIC FOOT-PLACEMENT STRATEGY SIMULATIONS. VALUES OF $y_{SEAT}$ AND $y_{SEAT}$ ARE IN METERS. THE VALUES OF OTHER VARIABLES ARE IN RADIANS.

| **Limb** | **Upper Limb** | | | | **Intact limb** | | | **Prosthetic limb** | | |
|---|---|---|---|---|---|---|---|---|---|---|
| **Coordinate** | $y_{\mathbf{seat}}$ | $y_{\mathbf{pelvis}}$ | $\theta_{\mathbf{pelvis}}$ | $\theta_{\mathbf{trunk}}$ | $\theta_{\mathbf{hip}}$ | $\theta_{\mathbf{knee}}$ | $\theta_{\mathbf{ankle}}$ | $\theta_{\mathbf{hip}}$ | $\theta_{\mathbf{knee}}$ | $\theta_{\mathbf{ankle}}$ |
| **Magnitude** | 0.500 | 0.638 | -0.227 | -0.546 | 1.39626 | -1.74533 | 0.576 | 1.362 | -1.689 | 0.608 |

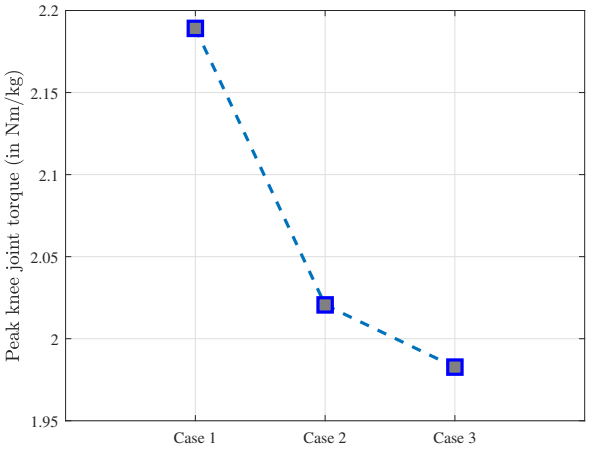


Fig. 12. Peak intact leg knee torque resulting from all the three cases of foot placement SiSt strategies. Case 1 - Asymmetric strategy with intact leg behind the prosthetic leg. Case 2 - Symmetric strategy with intact leg adjacent to the prosthetic leg. Case 3 - Asymmetric strategy with intact leg in front of the prosthetic leg.

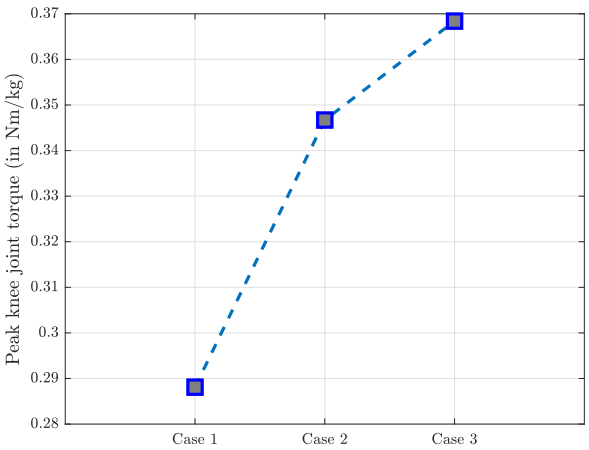


Fig. 13. Peak prosthetic leg knee torque resulting from all the three cases of foot placement SiSt strategies. Case 1 - Asymmetric strategy with intact leg behind the prosthetic leg. Case 2 - Symmetric strategy with intact leg adjacent to the prosthetic leg. Case 3 - Asymmetric strategy with intact leg in front of the prosthetic leg.

the prosthetic knee from when the prosthetic limb is placed adjacent to the healthy limb. Case 1 caused a 77% and 11% of asymmetry in knee and hip torques between the two limbs.

The peak hip torques on both sides are also plotted to observe its trend as the foot placement strategy moves from case 1 to case 3. An increment trend is observed in the hip torques on the intact side as the foot placement strategy is shifted from case 1 to case 3. Figure 14 illustrates this behaviour. The leap in hip torques from case 1 to case 2 is substantially smaller ($\approxeq$ 0.47%) as compared to the shift from case 2 to case 3 ($\approxeq$ 4.2%). The prosthesis side hip torque illustrates a different trend where symmetric foot placement yields the lowest peak torque value. Figure 15 shows the trend in the hip torques on the intact side. Placing the prosthetic foot forward still produces a lower torque value when compared to placing the prosthesis in front of the intact leg. However, having a symmetric foot placement produces the lowest torque value compared to the other two cases.

### *C. SiSt task simulation with a unilateral transfemoral amputee model with symmetric foot placement to test the effect of reduced weight-bearing asymmetry*

The SiSt task in able-bodied individuals is performed by loading both the limbs with marginal asymmetry. This weight-loading asymmetry is substantially higher in transfemoral am-

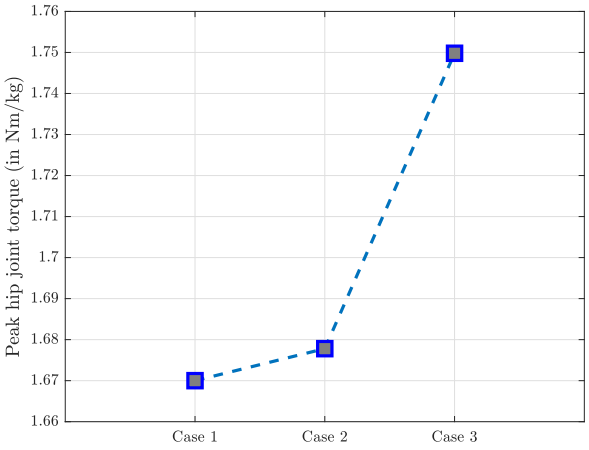


Fig. 14. Peak intact leg hip torque resulting from all the three cases of foot placement SiSt strategies. Case 1 - Asymmetric strategy with intact leg behind the prosthetic leg. Case 2 - Symmetric strategy with intact leg adjacent to the prosthetic leg. Case 3 - Asymmetric strategy with intact leg in front of the prosthetic leg.

TABLE V

PEAK KNEE TORQUES AND THEIR ASSOCIATED DOA ARISING FROM STANDING-UP WITH DIFFERENT FOOT PLACEMENT STRATEGIES. CASE 1 - ASYMMETRIC STRATEGY WITH INTACT LEG BEHIND THE PROSTHETIC LEG. CASE 2 - SYMMETRIC STRATEGY WITH INTACT LEG ADJACENT TO THE PROSTHETIC LEG. CASE 3 - ASYMMETRIC STRATEGY WITH INTACT LEG IN FRONT OF THE PROSTHETIC LEG.

| | **Case 1** | | **Case 2** | | **Case 3** | |
|---|---|---|---|---|---|---|
| | **Peak knee torque** | **Peak hip torque** | **Peak knee torque** | **Peak hip torque** | **Peak knee torque** | **Peak hip torque** |
| **Intact side** | 2.19 Nm/kg | 1.67 Nm/kg | 2.02 Nm/kg | 1.68 Nm/kg | 1.98 Nm/kg | 1.7498 Nm/kg |
| **Prosthesis side** | 0.29 Nm/kg | 1.33 Nm/kg | 0.35 Nm/kg | 0.51 Nm/kg | 0.37 Nm/kg | 0.7933 Nm/kg |
| **DoA** | 77% | 11% | 70% | 53% | 68% | 37% |

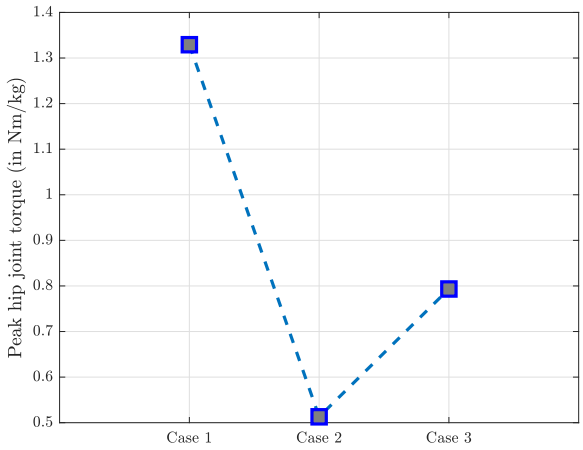


Fig. 15. Peak prosthetic leg hip torque resulting from all the three cases of foot placement SiSt strategies. Case 1 - Asymmetric strategy with intact leg behind the prosthetic leg. Case 2 - Symmetric strategy with intact leg adjacent to the prosthetic leg. Case 3 - Asymmetric strategy with intact leg in front of the prosthetic leg.

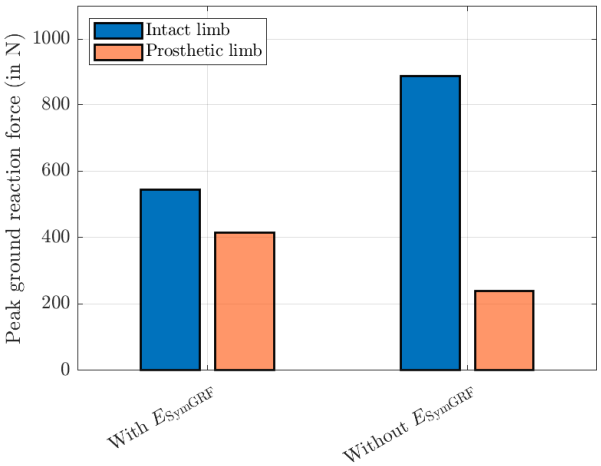


Fig. 16. Comparison of the peak ground reaction force in the intact and prosthetic limb resulting from the symmetric foot placement SiSt task simulation of a transfemoral amputee model with and without the implementation of $E_{\text{SymGRF}}$ term (this term is included to impose reduced weight-bearing condition).

putees [12]. A simulation experiment is designed to examine the effect of reduced asymmetry in the loading of both the limbs by a transfemoral amputee model while performing the SiSt task. Ground Reaction Force (GRF) is considered indicative of the load each limb bears. This experiment required the enforcement of the additional '$E_{\text{SymGRF}}$' objective function term (refer Equation 14) which ensured that the asymmetry in the GRF is reduced. The simulation scenario was similar to the earlier experiment with the able-bodied musculoskeletal model. Similar seat height and maximum duration were used. The muscle excitations were yet again parameterised with 10 control points separated by 0.12 s and initialised at 30% of their maximum capacities. Initial conditions pertaining to symmetric foot placement strategy (refer Table III) were configured for this experiment. The objective function was evaluated to test if all the objective function terms are rightly initialised and the optimisation was initiated.

Figure 16 shows the effect of including the '$E_{\text{SymGRF}}$' (refer 14) term in the objective function. The DoA in peak ground reaction forces greatly reduced from 57.4% observed in the experiment without the '$E_{\text{SymGRF}}$' term, to 13.4% to when this term was imposed.

The result of imposing such a condition in our simulation also reduced the peak intact knee torques by 13% as opposed to when this condition was not implied. This result is represented in Figure 17 and Table VI.

An increase in the peak hip torques on both the prosthesis side and intact side (7.1 % & 39% respectively) is observed as a consequence of imposing the reduced weight-bearing condition. This consequently increased the metabolic cost (computed using the '$E_{\text{effort}}$' term) needed to perform the SiSt task successfully. Figure 18 and 19 draws a comparison between the peak hip torques and metabolic costs which arise as a result of implementing the '$E_{\text{SymGRF}}$' term as opposed to when '$E_{\text{SymGRF}}$' term is not implemented. Figure 32 and 33 in Appendix G depicts the trend of the rate of metabolic energy as the movement became more symmetric.

Table VI enumerates the DoA in peak knee, hip and ground reaction forces arising from the implementation of the reduced weight-bearing condition.

The peak knee and hip torques resulting from the able-bodied model simulation is compared against peak knee and hip torques of the intact leg resulting from the implementation and non-implementation of '$E_{\text{SymGRF}}$' term. The results are tabulated in Table VII. The results for when the reduced weight-bearing condition was implied are more comparable to

TABLE VI

PEAK KNEE TORQUE, HIP TORQUES, GROUND REACTION FORCE AND THEIR ASSOCIATED DOA ARISING FROM THE IMPLEMENTATION OF THE REDUCED WEIGHT-BEARING CONDITION.

| | **With '$E_{\text{SymGRF}}$' term** | | | **Without '$E_{\text{SymGRF}}$' term** | | |
|---|---|---|---|---|---|---|
| | **Peak knee torque** | **Peak hip torque** | **Peak GRF** | **Peak knee torque** | **Peak hip torque** | **Peak GRF** |
| **Intact side** | 1.76 Nm/kg | 1.80 Nm/kg | 544 N | 2.02 Nm/kg | 1.68 Nm/kg | 886 N |
| **Prosthesis side** | 0.39 Nm/kg | 0.71 Nm/kg | 415 N | 0.35 Nm/kg | 0.51 Nm/kg | 240 N |
| **DoA** | 64% | 43% | 13% | 70% | 53% | 57% |

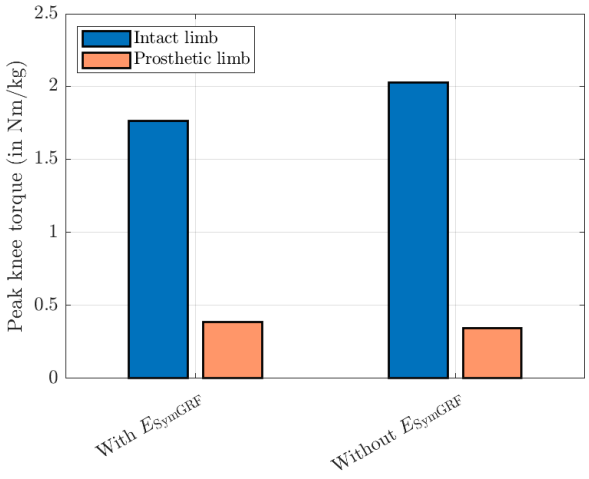


Fig. 17. Comparison of the peak knee torque in the intact and prosthetic limb resulting from the symmetric foot placement SiSt task simulation of a transfemoral amputee model with and without the implementation of $E_{\text{SymGRF}}$ term (this term is included to impose reduced weight-bearing condition).

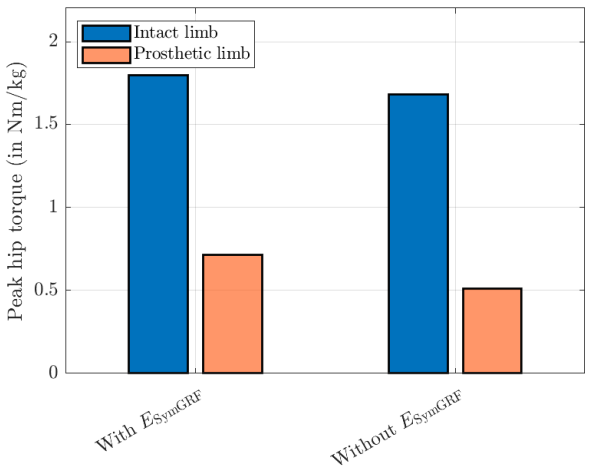


Fig. 18. Comparison of the peak hip torque in the intact and prosthetic limb resulting from the symmetric foot placement SiSt task simulation of a transfemoral amputee model with and without the implementation of $E_{\text{SymGRF}}$ term (this term is included to impose reduced weight-bearing condition).

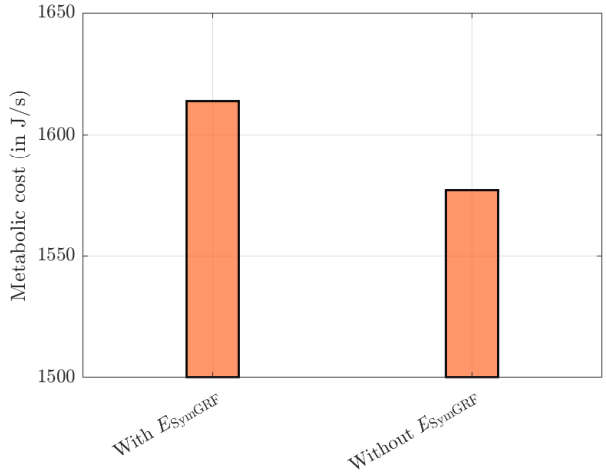


Fig. 19. Comparison of the metabolic cost resulting from the symmetric foot placement SiSt task simulation of a transfemoral amputee model with and without the implementation of $E_{\text{SymGRF}}$ term (this term to included to impose reduced weight-bearing condition).

TABLE VII

COMPARISON OF THE PEAK KNEE AND HIP TORQUES RESULTING FROM AN ABLE-BODIED MODEL SIST TASK SIMULATION AND TRANSFEMORAL AMPUTEE MODEL SIST TASK SIMULATION WITH AND WITHOUT REDUCED WEIGHT-BEARING ASYMMETRY CONDITION. NOTE: ONLY THE INTACT LIMB JOINT KINETICS OF THE TRANSFEMORAL AMPUTEE MODEL ARE COMPARED HERE.

| | **Peak knee torque (in Nm/kg)** | **Peak hip torque (in Nm/kg)** |
|---|---|---|
| **Able-bodied mode** | 1.37 | 1.17 |
| **Transfemoral amputee model (without reduced weight-bearing asymmetry condition)** | 2.02 | 1.68 |
| **Transfemoral amputee model (with reduced weight-bearing asymmetry condition)** | 1.76 | 1.80 |

the able-bodied model than the simulation where the condition was not implied.

## IV. Discussion

### A. On the sit-to-stand task simulation of an able-bodied model

The experiment with an able-bodied model aimed to compare the results of joint kinetics and kinematics reported in the literature with the simulation results and to verify the rightness of the simulation framework required to conduct other experiments.

Joint angle comparison plots show a reasonably good agreement with one another, thus ensuring that the SiSt task movement is proceeding in the right fashion.

Both the knee and hip joint torques resulted in a higher peak than the other studies. This result could be explained by a relatively short time duration observed in this simulation experiment. The study by Pai et al., (1991) [35] reports that a shorter movement time progressively increases the resulting knee joint torques and maintains roughly equal hip torques. Referring to Figure 10, it can be observed that Hutchinson et al., (1994) reports a shorter movement time than Doorenbosch et al., (1994) and Pai et al., (1991) and consequently results in a substantially higher peak knee moment. This argument, however, fails to explain the trend of the hip moment. Nonetheless, the peak hip moment value obtained through simulations reports a value much lower than the study by Bajd et al., (1982) [38] which reported a peak hip moment of 1.95 Nm/kg.

Other disparities observed through the results of this experiment may be accounted for by the fact that different authors might have used different environmental conditions, experimental setup or initial conditions to analyse the SiSt task movement.

The trends of the hip and knee joint angles and joint torques are comparable to the trends observed in the reviewed literature. Furthermore, the resulting peaks of the joint kinetics are comparable with reported values in literature. These results verify the rightness of the proposed simulation framework.

### B. On the effect of foot placement strategies on the sit-to-stand task simulation of a transfemoral amputee with active knee prosthesis

Three cases of foot placement were tested through the verified simulation framework to observe its effect on transfemoral amputee models enabled with active knee and passive ankle prosthesis.

It is seen from Figures 12 to 15 that the two configurations of asymmetrically placed feet have opposing effects. Results from Figure 13 indicated a greater contribution from prosthetic knee when placed behind the intact leg. The consequence of this is a reduced torque in the intact knee to successfully perform the SiSt task. The reduction was, however, not very substantial. The results are vice-versa when the feet exchange places.

Gillette et al., (2012) [6] reported an increase in knee extension torques of a posteriorly placed limb in a healthy able-bodied subject. Similar results were observed for a transfemoral amputee model, which showcased a reduced peak intact knee torque when it is placed in front of the prosthetic foot. An undesired consequence of this was an enormous increased hip extension torque on the intact side. Although the knee exerted a smaller torque, the hip compensated this by providing a higher torque.

The configuration demonstrated using case 3 satisfied the goal of reducing the effort of the intact knee in the SiSt task. Although the prosthesis provided a supporting torque, the DoA is still high (68%). The able-bodied model simulation have 0% DoA. The DoA was worse in asymmetric foot placement strategy performed with the intact leg behind the prosthetic leg with a value of 77%. Nevertheless, the asymmetric foot placement strategy with the intact leg in front of the prosthetic leg performed the best amongst the three cases.

In this case, the prosthetic limb was placed with initial knee flexion of 96 degrees and the healthy intact limb was placed at an initial knee angle of 85 degrees. A difference of about 10 degrees produces only a minute reduction in resultant knee moments. This result can be extrapolated to state that by placing the intact limb further apart from the prosthetic limb, a greater reduction can be expected. Also, using a prosthetic knee with higher torque limits will help reduce the intact limb knee effort.

It is noteworthy that in all three cases, the prosthetic knee did not use its torque delivering potential to its maximum. This behaviour is further examined in the next subsection.

### C. On the consequence of reducing weight-bearing asymmetry on the sit-to-stand task simulation of a transfemoral amputee with active knee prosthesis

Simulation involving a transfemoral amputee model with an active knee prosthesis was performed with an additional term enforcing the symmetric weight-bearing condition. The inclusion of this term increased the ground reaction force on the prosthetic limb and reduced the ground reaction force on the intact limb. Peak knee torques exhibited a similar trend as the peak GRFs. However, hip torques did not showcase a similar trend. The hip torques increased from when the condition of reduced weight-bearing symmetry was not implied.

An undesired repercussion of this increased hip torque was an increase in metabolic cost. This behaviour implied that, higher energy is required for a transfemoral amputee to perform the task by exerting more than the intended load on the prosthetic limb. Nevertheless, the peak intact knee joint torque was reduced and is now more comparable to the peak knee torque resulting from an able-bodied model simulation.

Although the hip torques on both sides (intact side and prosthesis side) increased, it is still within the agreeable range [34], [38]. A more symmetric motion was observed as a consequence.

It is also noteworthy that in the case when the condition of reduced weight-bearing asymmetry was not implied, the prosthetic knee did not work to its maximum potential and only produced 89% of its maximum torque capacity. The effect was also observed in hip torques on the prosthesis side, which was considerably small compared to when the reduced weight-bearing asymmetry was not applied. However, an implementation of the condition pushed both the prosthetic knee and to its limit and enhanced the performance of the hip on the prosthesis side. This behaviour could be explained

by the fact that the optimisation aimed to reduce metabolic cost amongst other terms when the '$E_{\text{SymGRF}}$' term is not applied and decreased the effort needed to perform the task by reducing the contribution from the prosthesis side. However, when the '$E_{\text{SymGRF}}$' term was later applied, a trade-off between minimising the metabolic cost and minimising the ground reaction force asymmetry needed to be found. Thus the optimiser might have chosen to increase the contribution from the prosthesis side to cater the '$E_{\text{SymGRF}}$' condition and also doing its best to reduce metabolic cost by still prioritising the intact limb more than the prosthetic limb.

### D. Limitations of this study

The primary limitation of this study is that all the actuation were restricted to the sagittal plane and hence cannot account for the actions in other planes. Baer et al., (1995) reports a considerable lateral movement of the trunk during the SiSt task [39]. Such additional degrees of freedom could improve the fidelity of the results.

The use of simplified musculoskeletal models also limited the results of this study. The human body is complex in terms of muscle properties and precision of joint movements. For example, the neck and head model is kept rigid and therefore, does not possess any degrees of freedom. However, it is common knowledge that the neck is a very compliant structure and therefore, could not be ideally assumed as rigid. It is believed that more accurate representations of the human body could have yielded better results. Nevertheless, a more comprehensive modelling of the musculoskeletal system could sometimes be redundant and may lead to unrealistic or overestimated solutions.

One of the major pitfalls of the simulations presented in this work is the sensitivity of the optimisation algorithm to the values of initiation parameters. A different set of initial parameter allocation leads to a different set of optimal solutions and makes it difficult to arrive the global solution.

Finally, the standing-up time observed from the able-bodied model SiSt simulation (0.790 s) is relatively short as compared to the actual movement time of the SiSt task reported in other studies (refer Figure 11). The implications of this have not been addressed in detail. It is believed that lenient vertical COM velocity constraints imposed on the objective function caused the optimiser to find a solution which has a short simulation time. A more narrow and strict COM velocity constraint could help solve the problem of short simulation times. Besides, a higher weight on the objective function term governing the effort could aid in minimising the energy needed to perform the SiSt task and consequently increase the simulation time. Pai et al., (1991) [35] has shown that standing-up time influences the kinetics of the SiSt task. Therefore, correcting for the simulation time might produce more comparable results.

## V. Recommendations

This section suggests two main recommendations to improve the results presented in this report.

The muscle excitation signal used in this work is parameterised using a piece-wise linear function. The use of such a function produces decent simulation responses. Nevertheless, several other functions could also be considered for this purpose. Appendix H describes an analysis conducted to deduce alternate functions to parameterise the muscle excitation signals. The analysis revealed that a cubic spline function could be used to represent the muscle excitation signals. However, these functions were not checked and could be a recommendation that could be extended in future works.

Another major improvement to this work could be achieved by adding an ankle actuator to the prosthesis. The current simulations involving the transfemoral amputee model are performed with a passive ankle. Simon et al., (2016) [14] has proved an ankle actuator could improve weight-bearing without having to exert more load on the prosthetic limb manually. Therefore, the current prosthetic model can be appended with an active torque generating ankle to provide a more controlled ankle torque. The simulation experiments in this study can be repeated with this modified model to observe the effect it will have on the joint moments of the intact limb.

## VI. Future Work

- Three-dimensional simulation: This work can be extended by adding additional degrees of freedom to the three-dimensional joints. A more complicated musculoskeletal model needs to be developed, which includes more muscles and therefore, more optimisation parameters. Having defined the objective function needed to perform the SiSt task, the experiments performed in this work can be repeated using the three-dimensional model to observe the contribution from the three-dimensional joints in reproducing a more realistic SiSt task. This study, however, has the disadvantage of increased computational effort.
- Effect of the residual limb: Length of the residual limb has significant effects on the performance of the hip joint on the amputated side of a transfemoral amputee. Therefore, it is logical to believe that it might have implications in the SiSt motion which requires a considerable hip torque. Hence, the analysis in this work should be repeated by including different lengths of the residual limb and consequently model its effect on the torque producing capabilities of the hip joint of the amputated side.
- Rehabilitation and therapeutic applications: A simulation study can have a variety of applications. The simulation framework proposed in this work can be used with a model mimicking the characteristics of a stroke patient or a paraplegic patient, and be used to the test rehabilitation techniques to promote the SiSt task. An optimisation study to device a typical SiSt manoeuvre using a patient-specific model could immensely improve the process of rehabilitation. Such studies could aid in engineering rehabilitation devices such as exoskeletons and assistive robots.
- Other determinants of SiSt task manoeuvre: The SiSt task manoeuvre has a number of determinants as summarised

in [5]. Therefore, it is possible that asymmetric foot placement strategy is not the only solution to reducing the efforts on the healthy knee of a transfemoral amputee. The simulation framework proposed in this work could be used to search other solutions to the same problem.

## VII. Conclusion

Increased effort by the healthy intact limb of a transfemoral amputee have serious short term and long term health implications for the amputee. In addition, the mobility can also affected if the amputee is not able to stand-up because of increased effort by the intact limb. It was proposed that using a support torque from an active knee prosthesis in combination with strategies like foot placement or reduced weight-bearing asymmetry could eliminate this problem. These conditions were tested using a predictive forward dynamic simulation methodology. Musculoskeletal models were developed in OpenSim, and the optimisation and simulation framework was set up in SCONE software.

Three cases were tested using the developed models and simulation framework. The results from the first experiment with an able-bodied model verified the framework developed for simulating the SiSt task. The results of the second experiment tested the effects of asymmetric foot placement on the joint torques. The third experiment with the same model as the second experiment tested the effect of reduced weight-bearing asymmetry.

Based on the reviewed literature, it was expected that the posterior prosthetic knee would exert more torque than usual, thus reducing the torques produced by the intact knee. This strategy has been proven to work in able-bodied individuals [6]. This work was essential to test the same for a transfemoral amputee with active knee prosthesis. This work proposed that an asymmetric foot placement strategy in combination with the support torque from the prosthetic knee could be used to reduce the torque produced the intact knee. Placing the prosthetic leg in front of the healthy leg performed badly by producing 77% DoA. The peak intact knee torque reduced when the prosthetic leg was placed behind the intact leg. The torque produced by the intact knee only reduced by 1.5% from when the intact leg is placed adjacent to the prosthetic leg. This cause a difference of only 2% in the DoA. Therefore, it can concluded that, although the intact knee torque and DoA reduces by placing the intact limb in front of the prosthetic leg rather than placing them adjacent to each other, the reduction is not substantial.

Another recommendation to reduce the effort of the healthy intact knee in transfemoral amputees with active knee prosthesis is to reduce the weight-bearing asymmetry that is prominent in transfemoral amputees. By reducing the weight-bearing asymmetry from 57% to 13% peak intact knee torques decreased by a considerable amount (13%). The peak knee torques as compared to an able-bodied model was only 28% more. Moreover, application of reduced weight-bearing asymmetry decreased the DoA in the peak knee torques from 70% to 64%. However, this increased the cost on metabolic energy needed to perform the SiSt task.

Both proposed strategies were successful in achieving the goal of reducing the torque in the intact knee. However, both strategies have their pitfalls. Comparing both the strategies to the symmetric foot placement simulation of the transfemoral model without the implementation of $E_{\text{SymGRF}}$ term, the strategy of placing the intact leg forward slightly reduces the peak knee torque in the intact leg (1.5%) but reduces the peak torque produced by the hip joints on the intact side. On the other hand, the reduced weight-bearing symmetry strategy has a greater influence on the reduction of the peak intact knee torque (13%) but consequently increases the peak torque produced by the hip joints on the intact side. This resulted in an increased metabolic cost.

Possible limitations of this work were discussed, and recommendations were provided to tackle the mentioned issues.

This work has demonstrated that other strategies exists to alleviate the problem of increased effort by the intact limb in a transfemoral amputee while performing the SiSt task. It is possible to adapt the simulation framework delineated in this work according to different test scenarios and simulate alternative SiSt manoeuvres.

## References


[1] T. Everett and C. Kell, *Human movement : An Introductory Text*, 6th ed. Edinburgh: Churchill Livingstone/Elsevier, 2010.

[2] M. F. Bobbert, D. A. Kistemaker, M. A. Vaz, and M. Ackermann, "Searching for strategies to reduce the mechanical demands of the sit-to-stand task with a muscle-actuated optimal control model," *Clinical Biomechanics*, vol. 37, pp. 83–90, 2016.

[3] H. Burger, J. Kuzˇelicˇki, and C. Marincˇek, "Transition from sitting to standing after trans-femoral amputation," *Prosthetics and Orthotics International TA - TT -*, vol. 29, no. 2, pp. 139–151, 2005.

[4] S. Özyürek, I. Demirbüken, and S. Angin, "Altered movement strategies in sit-to-stand task in persons with transtibial amputation," *Prosthetics and Orthotics International*, vol. 38, no. 4, pp. 303–309, sep 2013.

[5] W. G. M. Janssen, H. B. J. Bussmann, and H. J. Stam, "Determinants of the Sit-to-Stand Movement: A Review," *Physical Therapy*, vol. 82, no. 9, pp. 866–879, sep 2002.

[6] J. C. Gillette and C. A. Stevermer, "The effects of symmetric and asymmetric foot placements on sit-to-stand joint moments," *Gait and Posture*, vol. 35, no. 1, pp. 78–82, 2012.

[7] M. A. Hughes, D. K. Weiner, M. L. Schenkman, and R. M. Long, "Chair rise strategies in the elderly," *Clinical Biomechanics TA - TT -*, vol. 9, no. 3, pp. 187–192, 1994.

[8] W. Mathiyakom, J. L. McNitt-Gray, P. Requejo, and K. Costa, "Modifying center of mass trajectory during sit-to-stand tasks redistributes the mechanical demand across the lower extremity joints," *Clinical Biomechanics*, vol. 20, no. 1, pp. 105–111, 2005.

[9] S. J. Fleckenstein, R. L. Kirby, and D. A. MacLeod, "Effect of limited knee-flexion range on peak hip moments of force while transferring from sitting to standing," *Journal of Biomechanics*, vol. 21, no. 11, pp. 915–918, 1988.

[10] S. Kawagoe, N. Tajima, and E. Chosa, "Biomechanical analysis of effects of foot placement with varying chair height on the motion of standing up," *Journal of Orthopaedic Science*, vol. 5, no. 2, pp. 124–133, 2000.

[11] D. Brunt, B. Greenberg, S. Wankadia, M. A. Trimble, and O. Shechtman, "The effect of foot placement on sit to stand in healthy young subjects and patients with hemiplegia," *Archives of Physical Medicine and Rehabilitation*, vol. 83, no. 7, pp. 924–929, 2002.

[12] J. Kuželički, M. Žefran, H. Burger, and T. Bajd, "Synthesis of standing-up trajectories using dynamic optimization," *Gait & Posture*, vol. 21, no. 1, pp. 1–11, 2005.

[13] M. J. Highsmith, J. T. Kahle, S. L. Carey, D. J. Lura, R. V. Dubey, K. R. Csavina, and W. S. Quillen, "Kinetic asymmetry in transfemoral amputees while performing sit to stand and stand to sit movements," *Gait and Posture*, vol. 34, no. 1, pp. 86–91, 2011.

[14] A. M. Simon, N. P. Fey, K. A. Ingraham, S. B. Finucane, E. G. Halsne, and L. J. Hargrove, "Improved Weight-Bearing Symmetry for Transfemoral Amputees During Standing Up and Sitting Down With a Powered Knee-Ankle Prosthesis," *Archives of Physical Medicine and Rehabilitation*, vol. 97, no. 7, pp. 1100–1106, 2016.

[15] T. M. Lundin, M. D. Grabiner, and D. W. Jahnigen, "On the assumption of bilateral lower extremity joint moment symmetry during the sit-to-stand task," *Journal of Biomechanics*, vol. 28, no. 1, pp. 109–112, 1995. [Online]. Available: http://www.sciencedirect.com/science/article/pii/0021929095800131

[16] M. W. Rodosky, T. P. Andriacchi, and G. B. J. Andersson, "The influence of chair height on lower limb mechanics during rising," *Journal of Orthopaedic Research*, vol. 7, no. 2, pp. 266–271, mar 1989. [Online]. Available: https://doi.org/10.1002/jor.1100070215

[17] J. Wang, S. Hamner, S. Delp, and V. Koltun, "Optimizing Locomotion Controllers Using Biologically-Based Actuators and Objectives." *ACM transactions on graphics TA - TT -*, vol. 31, no. 4, 2012.

[18] A. Seth, J. Hicks, T. Uchida, A. Habib, J. Dunne, C. Ong, M. Millard, S. Lakshmikanth, M. Sherman, J. Ku, S. Delp, C. Dembia, M. DeMers, A. Rajagopal, S. Hamner, E. Arnold, and J. Yong, "OpenSim: Simulating musculoskeletal dynamics and neuromuscular control to study human and animal movement," *PLoS Computational Biology*, vol. 14, no. 7, 2018.

[19] T. Geijtenbeek, "SCONE: Open Source Software for Predictive Simulation of Biological Motion," *Journal of Open Source Software*, vol. 4, no. 38, p. 1421, 2019.

[20] M. Christophy, N. A. Faruk Senan, J. C. Lotz, and O. M. O'Reilly, "A Musculoskeletal model for the lumbar spine," *Biomechanics and Modeling in Mechanobiology*, vol. 11, no. 1, pp. 19–34, 2012. [Online]. Available: https://doi.org/10.1007/s10237-011-0290-6

[21] A. N. Vasavada, S. Li, and S. L. Delp, "Influence of muscle morphometry and moment arms on the moment-generating capacity of human neck muscles," *Spine*, vol. 23, no. 4, pp. 412–422, 1998.

[22] M. Millard, T. Uchida, A. Seth, and S. L. Delp, "Flexing Computational Muscle: Modeling and Simulation of Musculotendon Dynamics," *Journal of Biomechanical Engineering*, vol. 135, no. 2, feb 2013.

[23] P. J. Millington, B. M. Myklebust, and G. M. Shambes, "Biomechanical analysis of the sit-to-stand motion in elderly persons," *Archives of Physical Medicine and Rehabilitation*, vol. 73, no. 7, pp. 609–617, 1992.

[24] A. A. o. O. Surgeons., "Joint motion : method of measuring and recording." Chicago, 1965.

[25] K. H. Hunt and F. R. E. Crossley, "Coefficient of Restitution Interpreted as Damping in Vibroimpact," *Journal of Applied Mechanics*, vol. 42, no. 2, pp. 440–445, jun 1975.

[26] L. A. Gilchrist and D. A. Winter, "A two-part, viscoelastic foot model for use in gait simulations," *Journal of Biomechanics*, vol. 29, no. 6, pp. 795–798, 1996.

[27] A. Pérez-González, C. Fenollosa-Esteve, J. L. Sancho-Bru, F. T. Sánchez-Marín, M. Vergara, and P. J. Rodríguez-Cervantes, "A modified elastic foundation contact model for application in 3D models of the prosthetic knee," *Medical Engineering & Physics*, vol. 30, no. 3, pp. 387–398, 2008.

[28] E. Linder-Ganz, N. Shabshin, Y. Itzchak, and A. Gefen, "Assessment of mechanical conditions in sub-dermal tissues during sitting: A combined experimental-MRI and finite element approach," *Journal of Biomechanics*, vol. 40, no. 7, pp. 1443–1454, 2007.

[29] H. A. Varol, F. Sup, and M. Goldfarb, "Powered sit-to-stand and assistive stand-to-sit framework for a powered transfemoral prosthesis," in *2009 IEEE International Conference on Rehabilitation Robotics, ICORR 2009*, 2009, pp. 645–651.

[30] P. L. Weiss, R. E. Kearney, and I. W. Hunter, "Position dependence of ankle joint dynamicsâI. Passive mechanics," *Journal of Biomechanics*, vol. 19, no. 9, pp. 727–735, 1986.

[31] N. Hansen, "The CMA Evolution Strategy: A Comparing Review BT - Towards a New Evolutionary Computation: Advances in the Estimation of Distribution Algorithms," J. A. Lozano, P. Larrañaga, I. Inza, and E. Bengoetxea, Eds. Berlin, Heidelberg: Springer Berlin Heidelberg, 2006, pp. 75–102.

[32] T. Geijtenbeek, A. Van Der Stappen, and M. Van De Panne, "Flexible muscle-based locomotion for bipedal creatures," *ACM Transactions on Graphics TA - TT -*, vol. 32, no. 6, 2013.

[33] M. E. Roebroeck, C. A. M. Doorenbosch, J. Harlaar, R. Jacobs, and G. J. Lankhorst, "Biomechanics and muscular activity during sit-to-stand transfer," *Clinical Biomechanics*, vol. 9, no. 4, pp. 235–244, 1994.

[34] C. A. M. Doorenbosch, J. Harlaar, M. E. Roebroeck, and G. J. Lankhorst, "Two strategies of transferring from sit-to-stand; The activation of monoarticular and biarticular muscles," *Journal of Biomechanics*, vol. 27, no. 11, pp. 1299–1307, 1994.

[35] M. Pai and Y. Rogers, "Speed variation and resultant joint torques during sit-to-stand," *Archives of Physical Medicine and Rehabilitation*, vol. 72, no. 11, pp. 881–885, 1991.

[36] S. Bajelan and A. MR, "Musculoskeletal modeling and simulation of three various Sit-to-Stand strategies: An evaluation of the biomechanical effects of the chair-rise strategy modification." *Technology and health care : official journal of the European Society for Engineering and Medicine TA - TT -*, vol. 22, no. 4, pp. 627–644, 2014.

[37] E. B. Hutchinson, P. O. Riley, and D. E. Krebs, "A dynamic analysis of the joint forces and torques during rising from a chair," *IEEE Transactions on Rehabilitation Engineering*, vol. 2, no. 2, pp. 49–56, 1994.

[38] T. Bajd, A. Kralj, and R. Turk, "Standing-up of a healthy subject and a paraplegic patient," *Journal of Biomechanics*, vol. 15, no. 1, pp. 1–10, 1982.

[39] B. GD and A. AM, "Trunk movements in older subjects during sit-to-stand." *Archives of physical medicine and rehabilitation TA - TT -*, vol. 76, no. 9, pp. 844–849, 1995.

[40] J. J. Visser, J. E. Hoogkamer, M. F. Bobbert, and P. A. Huijing, "Length and moment arm of human leg muscles as a function of knee and hip-joint angles," *European Journal of Applied Physiology and Occupational Physiology*, vol. 61, no. 5-6, pp. 453–460, 1990.

[41] G. Németh and H. Ohlsén, "In vivo moment arm lengths for hip extensor muscles at different angles of hip flexion," *Journal of Biomechanics*, vol. 18, no. 2, pp. 129–140, 1985.

[42] A. J. van Soest and M. F. Bobbert, "The contribution of muscle properties in the control of explosive movements," *Biological Cybernetics*, vol. 69, no. 3, pp. 195–204, 1993.

[43] C.-C. Liang and C.-F. Chiang, "A study on biodynamic models of seated human subjects exposed to vertical vibration," *International Journal of Industrial Ergonomics*, vol. 36, no. 10, pp. 869–890, 2006.

[44] M. Emadi Andani, F. Bahrami, P. Jabehdar Maralani, and A. J. Ijspeert, "MODEM: a multi-agent hierarchical structure to model the human motor control system," *Biological Cybernetics*, vol. 101, no. 5, pp. 361–377, 2009.

[45] V. Norman-Gerum and J. McPhee, "Constrained Dynamic Optimization of Sit-to-Stand Motion Driven by Bézier Curves," *Journal of Biomechanical Engineering*, vol. 140, no. 12, oct 2018.

[46] R. R. Coermann, "The Mechanical Impedance of the Human Body in Sitting and Standing Position at Low Frequencies," *Human Factors: The Journal of Human Factors and Ergonomics Society*, vol. 4, no. 5, pp. 227–253, 1962.

[47] M. G. Pandy, M. G. Pandy, and F. C. Anderson, "Optimal Control of Non-ballistic Muscular Movements: A constraint-based performance criterion for rising from a chair," *Journal of Biomechanical Engineering*, vol. 117, no. 1, pp. 15–26, 1995.

[48] M. W. Hast, B. G. Hanson, and J. R. Baxter, "Simulating contact using the elastic foundation algorithm in opensim," *Journal of Biomechanics*, vol. 82, pp. 392 – 396, 2019.

[49] F. C. Anderson, "A dynamic optimization solution for a complete cycle of normal gait," Ph.D. dissertation, 1999.

[50] L. J. Bhargava, M. G. Pandy, and F. C. Anderson, "A phenomenological model for estimating metabolic energy consumption in muscle contraction," *Journal of Biomechanics*, vol. 37, no. 1, pp. 81–88, 2004.

[51] R. Shadmehr, S. P. Wise, S. P. Wise *et al.*, *The computational neurobiology of reaching and pointing: a foundation for motor learning*. MIT press, 2005.

## APPENDIX

### A. SiSt task overview

The sit-to-stand (SiSt) task involves guiding the centre of mass (COM) from a stable quite-sitting posture to a stable quite-standing posture. This is one of the most energy-consuming daily tasks as it involves doing work against the will of gravity. The torques generated by the lower limb joints (hip, knee and the ankle) dominate the task along with adequate help from the upper limb trunk segments. The task begins with an initiation phase where the trunk begins to flex, thereby generating the moment needed to rise the COM. This is followed by a seat-unloading phase where the body unloads

from the seat (seat-off instance) by virtue of the momentum generated by the trunk and the torques produced at the hip and the knee. The knee and hip continue to provide the torque while the trunk adjusts itself to reach a standing posture in the ascension phase. Once the body reaches the desired posture, it stabilises itself by slightly swaying back and forth. The task then ends with a steady quite standing pose. Figure 20 pictorially represents the SiSt task.

Several strategies are used to bring about the said motion. Amongst them, three strategies are prominent. These are The Momentum transfer (MT) strategy, The Dominant Vertical Rise (DVR) strategy and the Exaggerated Trunk Flexion (ETF) strategy. These strategies mainly differ in the extent of trunk flexion and the effort required by the lower-body segmental joints (mainly the hip and knee). These strategies are further delineated as follows.

The MT strategy, regarded as the normal strategy, uses the trunk segment to first generate sufficient momentum by flexing forward, thereby generating the part of the energy needed to stand up. The lower body segmental joints provide the residual energy to raise the centre of mass (COM) to the desired quite-standing position. The generated momentum assists the lower body in performing the SiSt task using the MT strategy.The COM transitions through some unstable phases during this strategy. However, the momentum generated by the trunk during the initial phase of the movement ensures that the COM transitions through these unstable postures quickly, thus maintaining the overall stability and preventing any imbalance that might occur.

The ETF strategy first involves positioning the COM over the feet by flexing the trunk further front and attaining the standing posture by raising the COM by virtue of the lower limb segmental joints. This movement strategy is regarded as more stable due to the absence of unstable phases which are part of the MT strategy. The COM resides within the base of support (BOS) throughout the motion. The surface of the feet constitutes the base of support. The ETF strategy loads the lower limb joints more than the MT strategy due to the absence of the trunk momentum. This strategy is observed in elderly subjects who lack the strength to generate the momentum needed to rise up and because they prioritise stability over effort. However, lower muscle strengths in elderly subjects pose a limitation to this strategy and lead to greater effort.

The DVR strategy displays the least trunk flexion amongst the strategies. The lower limb takes the greatest toll on this strategy. The torques generated by the hip, knee, and ankle are solely responsible for raising the COM to the desired standing-up posture due to the absence of momentum generated by the trunk and also transitioning the COM through the unstable phases that occur during the motion. Thus, the DVR becomes the most energy-consuming strategy amongst all the strategies.

### *B. Musculoskeletal model details*

*1) Model Topology:* The pelvis is defined with respect to the ground and consists of three degrees of freedom. It is allowed to translate horizontally and vertically and is allowed to rotate about the third axis. The hip, knee and ankle joints are modelled as one degree of freedom hinge joints which are allowed to rotate only about the sagittal plane.

The trunk segment plays a significant role in the SiSt task. This required the trunk segment to be modelled as close to a biological human trunk as possible. The model was modified to decompose the trunk into six segments. This modified trunk segment has bodies representing L1-L5 segments of the lumbar spine region and a body representing the thoracic region connected with one degree of freedom hinge joints. The neck and the skull segments were rigidly attached to the thoracic segment and thus did not possess any degrees of freedom. The joint responsible for trunk flexion forms the intersection between L5 and sacrum (L5-S1). Other joints of the lumbar spine segment (L5-L4, L4-L3, L3-L2, L2-L1) are constrained to move in accordance with the L5-S1 joint. These other coordinates are coupled with the L5-S1 joint through a linear relation. Actuation of the L5-S1 joint actuates the other four lumbar joints.

Each of the 22 segments of the model is provided with a mass and has a moment of inertia defined in all nine directions. Every segment has a separate or group of geometry files associated with it. These files helped visualise the segments.

The process of constructing the musculoskeletal model of an able-bodied model followed the topology depicted in Figure 21.

*2) Musculotendon model:* The musculoskeletal model consists of a total of 20 muscles which includes 16 lower limb muscles and 4 upper limb muscles. This subsection gives a brief overview of the musculotendon element and its actuation as delineated in the article by Millard et al., (2013) [22].

The torques generated at the joints are a function of two properties of the musculoskeletal system. The first property is the moment arm, which is a function of the joint angles and an inherent property of musculotendon attachment to the skeletal system. The second property pertains to the force deliverable by each musculotendon.

Muscle attachments points used in this work were already established in the sub-models used to construct the final model. These points were derived from human cadavers by measuring the distance of the points in all three principal directions relative to a reference point. The moment arm as a function of the joint angle was computed inherently using these attachment points by the OpenSim software.

Based on the knowledge of muscle function, an excitation signal needs to be sent from the brain to activate the muscles. Once it is activated, the muscle contracts to a particular length with a certain velocity in some delta time, thus outputting a force. This force is transmitted to the joints through the tendons which form a bridge between the muscles and the skeletal structure. Once a required actuation is complete, the muscle deactivates and returns to its dormant state. A set of mathematically defined equations describe these two main events. The event of activating the muscle through an excitation signal is defined using activation dynamics (equation 16), and the event of contraction of the musculotendon element is called contraction dynamics (equation 17).

The activation $a$, of a muscle used in this work, is defined as first-order differential equation as follows. For an excitation

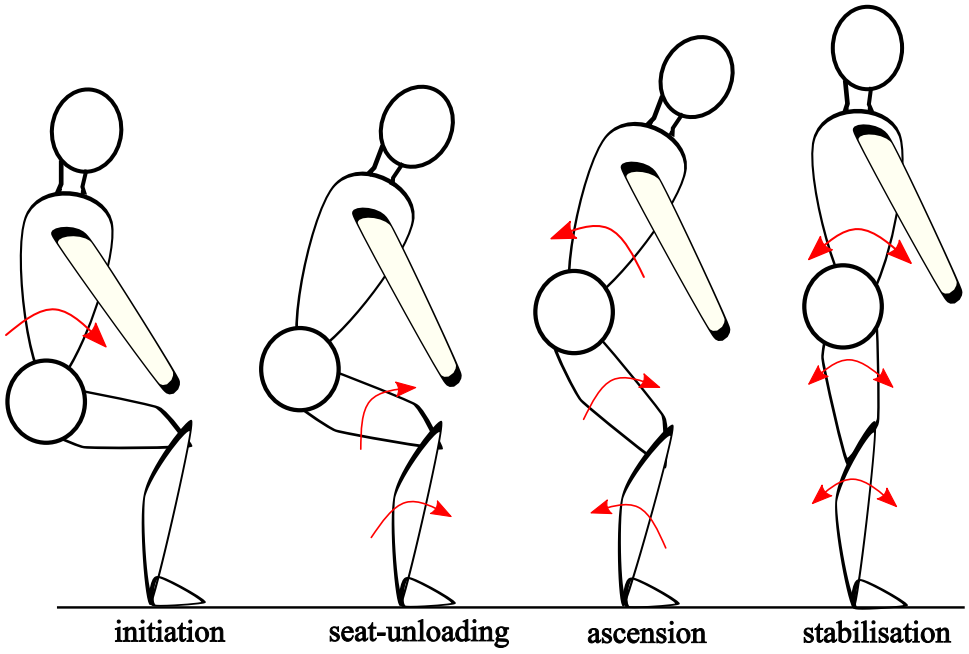


Fig. 20. Transition of the sit-to-stand task

signal $e$,

$$\frac{\mathrm{d}a}{\mathrm{d}t} = \tau(e - a). \tag{16}$$

Where $\tau$, is activation or deactivation time constant.

The contraction dynamics is described using Figure 26. The musculotendon is simplified to a spring-damper system in order to derive the musculotendon force. The musculotendon consists of an active contractile element in parallel to a passive elastic element modelling a muscle, and an elastic tendon which together produce the force. Assuming the tendon to be elastic structure, an equilibrium is established between $f^{\mathrm{T}}$ and $f^{\mathrm{M}}$. The force resulting by solving equation 17 is transmitted to the joints.

$$(f_o^{\mathrm{M}}(af^{\mathrm{L}}(l^{\mathrm{M}})f^{\mathrm{V}}(v^{\mathrm{M}}) + f^{PE}(l^{\mathrm{M}}))\cos(\alpha)) - f_o^{\mathrm{M}}f^{\mathrm{T}}(l^{\mathrm{T}}) = 0 \tag{17}$$

Where,

$f_o^{\mathrm{M}}$ is the maximum isometric force that the muscle fibres can generate at an optimal fibre length $l_o^{\mathrm{M}}$,

$f^{\mathrm{L}}(l^{\mathrm{M}})$ is the fibre length dependent force outputted by the contractile element,

$f^{\mathrm{V}}(v^{\mathrm{M}})$ is the contraction velocity dependent force outputted by the contractile element,

$f^{\mathrm{PE}}(l^{\mathrm{M}})$ is the length dependent force outputted by the passive elastic element,

$\alpha$ is called the pennation angle. It is the relative angle between the muscle and the tendon which scales the force transmitted to the joint,

$a$ is the level of activation; $0.01 \leq a \leq 1$.

*3) Motivation behind inclusion of trunk muscles and changes to the muscle properties:* The choice of including the erector spinae and the rectus abdominis muscles is motivated by the fact that the iliopsoas (responsible for trunk flexion and extension in the original 9 DOF model) did not have substantially large moment arm to bring about the trunk flexion and extension. At a hip flexion between 60-80 degrees (the range of initial hip joint angle while sitting), the moment arm value is close to zero and is also not capable of producing sufficient force to cause a torque to flex the trunk. Thus, stronger muscles dedicated to trunk flexion and extension were included. Abdominal muscles and back muscles were chosen for this task.

The muscle properties were modified to suit the requirements of the SiSt task. The approach is delineated as follows. For the sake of distinguishability, the term "original model" will be used to describe the old model (the 9-DOF model in SCONE) with old parameters and the term "modified model" will be used to describe the new model with modified parameters. These terms will be just used in this subsection and will not be carried forward.

The moment producing capabilities rely on the moment arm and force deliverable by the muscle. An inspection of these properties of the original model was checked to see if it were capable of generating the required moment to bring about the SiSt motion.

The moment arm information as a function of joint angle of the muscle responsible for hip and knee joint actuation were extracted from the original model and compared to moment arm data available in the literature. The data from literature were reported by experimentally measuring the moment arm by varying the joint angles of a human cadaver [40], [41]. Gastrocnemius, Rectus Femoris and Vasti are responsible for knee joint actuation whereas, Hamstring, Bicep Femoris, Gluteus Maximum and Iliopsoas are responsible for hip joint actuation. The moment arm information pertaining to Vasti, Iliopsoas and bicep femoris were not readily available in the literature and hence excluded from this comparison. The

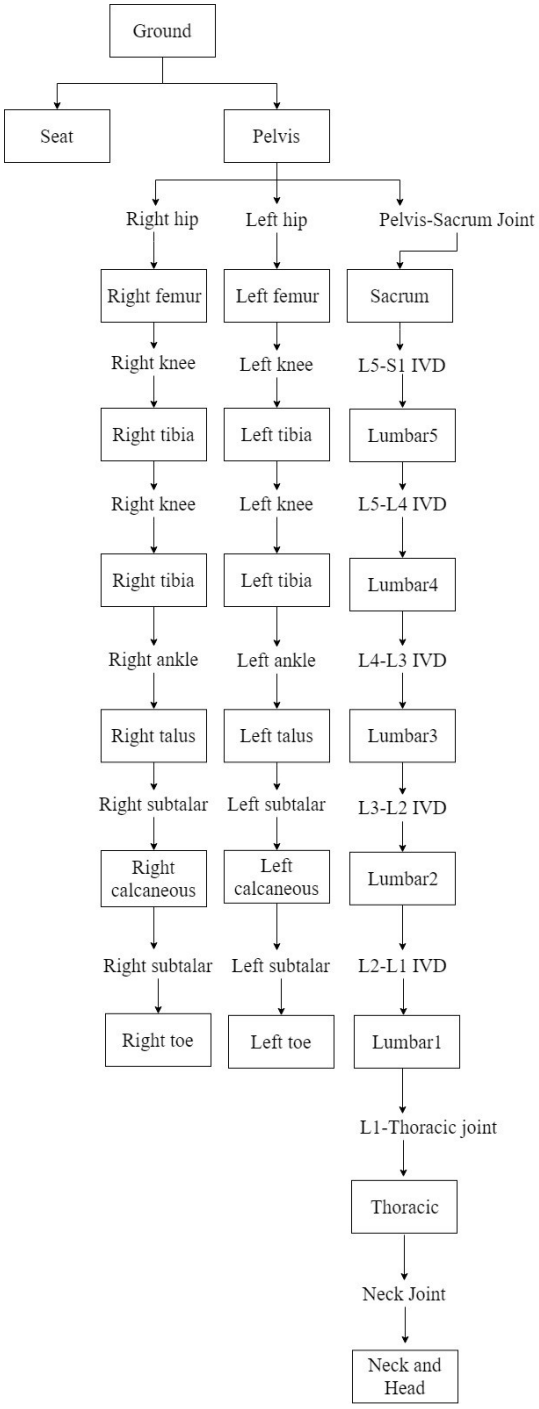


Fig. 21. Open-chain topology of the musculoskeletal model of an able-bodied individual.

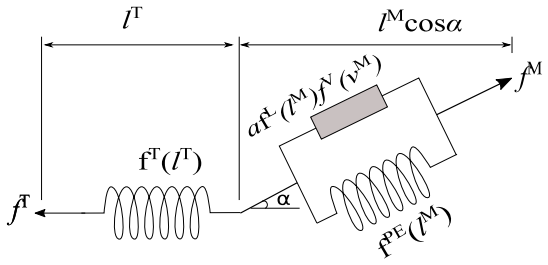


Fig. 22. Three-element Hill type Millard muscle model (Drawing inspired from [22]).

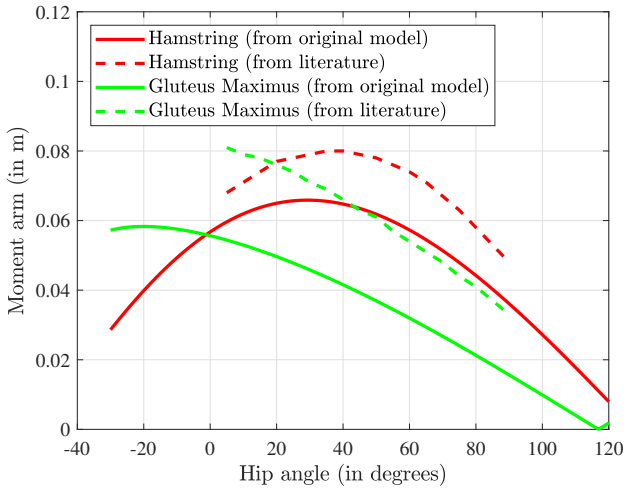


Fig. 23. Comparison plots of the hip muscle moment arms of the 9-DOF musculoskeletal model (model that pre-existed in SCONE) with the hip muscle moments arms derived from literature. The data is referred from [40], [41].

comparison plots are depicted in Figure 23 and 24.

Figures 24 illustrate comparable moment arm variation for the knee joint. However, the moment arm variation of the hip joint is not comparable, as illustrated in Figure 23. Nevertheless, a tangible conclusion could not be drawn without examining the force deliverable by the muscles.

A similar comparison study was conducted to test the maximum isometric force produced by the hip and knee muscles. The caparison was made against a model developed by van Soest et al., (1993) [42], which was used in some simulation studies, including a simulation of the SiSt motion [2]. The maximum isometric force information of the iliopsoas and bicep femoris was missing for this study and hence excluded from the comparison. The comparison plots are as follows.

There is a substantial difference in these muscle properties, which were not ideal for the simulation of the SiSt motion. The moment arm cannot be modified directly. Therefore the isometric muscle forces were modified in accordance with the model by van Soest et al., (1993) [42]. This revision of maximum isometric force solved the problems associated with moment generation.

Table VIII lists the values of muscle properties used in our musculoskeletal model.

*4) Ligament properties:* The stiffness and damping values of knee ligaments pre-existed in the original model and hence adopted in the modified model. The values of the hip joint ligament were adopted from the OpenSim models developed by the Stanford Neuromechanics Laboratory. Trunk ligament values had to be derived mathematically and added to the model.

As described in the model topology, the L5 segment governs the movement of the trunk segment. Therefore, a ligament was placed at the joint formed between the L5 and the sacrum (L5-S1 Intervertebral Disk or IVD). The following methodology was used to derive the stiffness value of the L5-S1 IVD

TABLE VIII
PROPERTIES OF THE MUSCULOTENDONS USED IN THE MUSCULOSKELETAL MODEL

| Muscle | Maximum Isometric Force (N) | Optimal Fiber Length (m) | Tendon Slack Length (m) | Pennation Angle (degrees) |
|---|---|---|---|---|
| **Hamstrings** | 4000 | 0.109 | 0.326 | 0 |
| **Gluteus Maximus** | 5000 | 0.147 | 0.127 | 0 |
| **Iliopsoas** | 2342 | 0.100 | 0.160 | 0.139 |
| **Rectus Femoris** | 3000 | 0.114 | 0.310 | 0.087 |
| **Vasti** | 9000 | 0.107 | 0.116 | 0.052 |
| **Gastrocnemius** | 4000 | 0.090 | 0.360 | 0.296 |
| **Soleus** | 8000 | 0.050 | 0.250 | 0.436 |
| **Tibialis Anterior** | 3000 | 0.098 | 0.223 | 0.087 |
| **Rectus Abdominis** | 348 | 0.210 | 0.016 | 0 |
| **Erector Spinae** | 2500 | 0.081 | 0.210 | 0.228 |

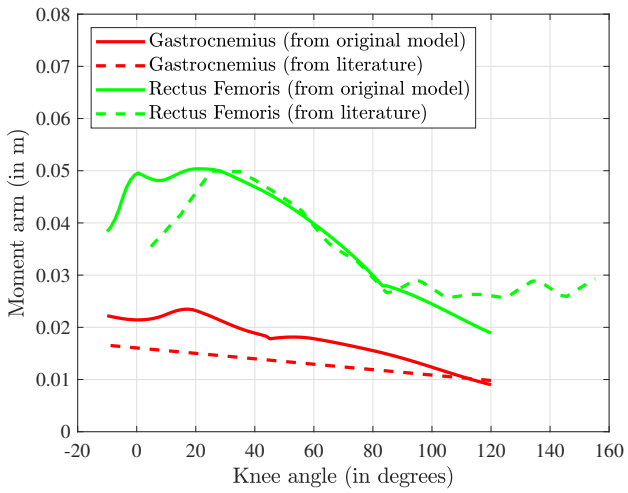


Fig. 24. Comparison plots of the knee muscle moment arms of the 9-DOF musculoskeletal model (model that pre-existed in SCONE) with the knee muscle moments arms derived from literature. The data is referred from [40], [41].

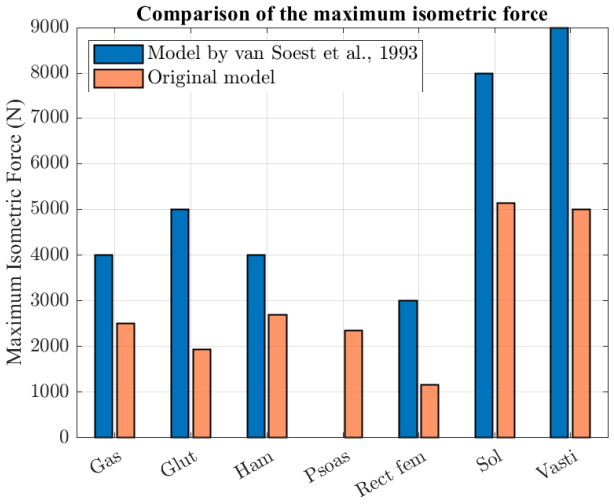


Fig. 25. Comparison plot of the maximum isometric muscle force of the original musculoskeletal model with the maximum isometric muscle force derived from the van Soest model [42].

ligament logically.

It was assumed that, at one degree greater than the flexion limit of the trunk, the body is in static equilibrium due to the virtue of the passive ligament forces. Considering this, a moment balance Equation was formed.

$$M_{\text{trunk}} = mglcos(\theta) \tag{18}$$

Where $M_{\text{trunk}}$ is the net moment of the trunk segment about the L5-S1 IVD joint, $m$ is the mass of the trunk in kilograms, $g$ is the acceleration due to gravity in m/s$^2$ and $\theta$ is trunk flexion angle in degrees.

For a trunk weighing 35 kgs, at and angle $31^o$ (one degree more than the flexion limit of $30^o$), a torque of 120.8 Nm/degree of torque is required to maintain equilibrium and thus this value is adopted as the stiffness of the L5-S1 ligament. Table IX tabulates the parameter values of the ligament elements.

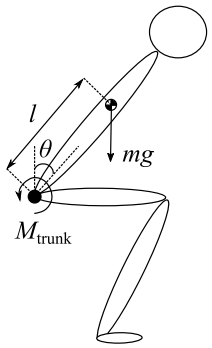


Fig. 26. Free-body diagram for calculating the moment exerted by the passive trunk ligament model.

### C. Contact models

Contact models help mathematically define interactions of the musculoskeletal model with the environment. Two inherent contact models are required for simulating the SiSt task. The

TABLE IX
PROPERTIES OF THE LIGAMENT MODELS INCORPORATED IN THE MUSCULOSKELETAL MODEL

| Location of the ligament | Stiffness (Nm/deg) | Damping (Nms/deg) |
|---|---|---|
| Knee | 2 | 0.2 |
| Hip | 200 | 0.2 |
| L5-S1 IVD | 115 | 0.2 |

first being the interaction of the foot with the ground and interaction of the buttocks with the seat.

The foot-ground contact model is represented using Hunt-Crossley model which based on Hertz contact theory [25], and the seat-buttocks contact model is represented using elastic foundation force based on the Elastic foundation theory [27]. These two theories presume the foundation (half-spheres) as a set of springs and dampers which produce resultant forces as a result of the deformation caused during contact. The bodies that are part of the musculoskeletal structures are modelled as spheres, and the environment in contact is modelled as half-spheres in this work. Figure 27 illustrates this interaction.

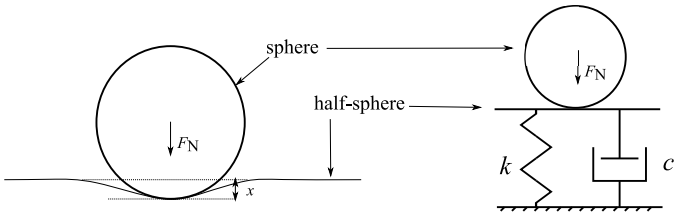


Fig. 27. Representation of the theory for computing the force, $F_N$. The dynamics of the half-sphere is modelled as a spring-damper system

The parameters needed to compute the forces between foot and the ground were already established in other studies [26] and already exited in the model library of SCONE.

The interaction between the buttocks and the seat needed further inspection. Existing literature was scanned to determine the type of contact model to be implemented in this work. Four contact models were observed in literature; however, the reason for the implementation of a particular model was not apparent. Table X lists the models inspected in this work. The following procedure was used to analyse and choose the right type of contact model.

Liang & Chiang [43] tabulated a measure called the Seat-to-Head transmissibility (STH) ratio by placing subjects on a vertically vibrating seat and measuring the resulting linear acceleration transmitted to the head as a ratio of the acceleration provided by the vibrating seat (equation 19). This experiment was conducted at multiple frequencies, and the results were tabulated. This approach was followed for analysing the seat-buttocks model as a framework to choose the appropriate model. The transmissibility ratio was computed, tabulated and plotted for a number of frequencies. The non-linear systems were numerically simulated using ode23 numerical integrator. Horizontal components were not considered for analysis due to a lack of reference for comparison. Andani & Bahrami, 2009 [44] did not report the parameters for their model thus are excluded from this analysis. Figure 24 plots the results of this analysis.

$$TR = \frac{\ddot{y}_{\max}(t)}{\ddot{y}_0(t)} \tag{19}$$

Where $\ddot{y}_{max}(t)$ is the maximum acceleration value of the response for one particular frequency at steady-state and $\ddot{y}_0(t)$ is the amplitude of the acceleration of the excitation frequency. The ratio was calculated in the time domain rather than the frequency domain to deal with the presence of non-linearities.

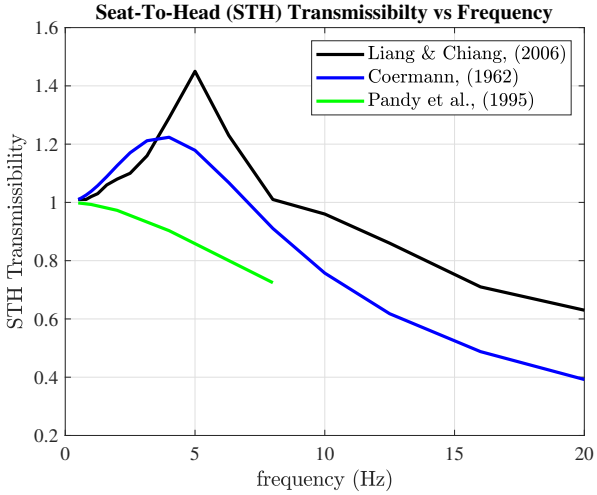


Fig. 28. Plot of STH Transmissibility Ratio vs Frequency for seat-body interaction models. Plot depicting Liang & Chiang, 2006 [43] is experimentally derived and used as reference for comparison.

A linear model works best based on the results of the above analysis. The seat-buttocks model was intended to be modelled using a linear model realising the results of the above analysis. Parameters of the contact model were computed using a linear model. This model was simulated for the frequencies mentioned in Liang & Chiang [43] and the STH transmissibility was computed (refer Figure 29). The parameters leading to the closest response as the experimental values were chosen to be incorporated in the final model. Figure 28 shows the results of the analysis.

OpenSim allows the use of only the Hunt-Crossley model [25] or Elastic Foundation model [27] to define the interaction with the environment. The two models in its original form are represented in Equation 1 and 2 were tried to fit with the experimentally obtained STH transmissibility. However, no feasible solution. Since it was not possible to define custom contact models in OpenSim, it was decided to use the best possible alternative. The stiffness component was linear in the elastic foundation model, and the damping term did not have very drastic effects on the dynamics of the motion, and therefore, this was a more appropriate choice. Figure 30 shows the comparison between experimental data and the fitted linear model. A sphere of the radius mentioned in [28] and mesh information from [48] was constructed and implemented in the model.

TABLE X
SEAT-BUTTOCKS INTERACTION MODELS OBSERVED IN LITERATURE

| # | Author | DOF | Seat-buttocks Interaction Model | Nomenclature |
|---|---|---|---|---|
| 1. | Norman-Gerum & McPhee, 2018 [45] | 1 | $\sigma = E\epsilon + \eta\dot{\epsilon}$ | $\sigma-$ Stress,<br>$\epsilon-$ Strain,<br>E$-$ Modulus of elasticity<br>$\eta-$ Viscosity |
| 2. | Coermann, 1962 [46] | 1 | $F_y = K\triangle y + B\triangle\dot{y}$ | K $-$ Stiffness<br>B $-$ Damping<br>$\triangle y-$ Net vertical displacement<br>$\triangle\dot{y}-$ Vertical velocity |
| 3. | Andani & Bahrami, 2009 [44] | 2 | $F_y = \begin{cases} [K - B(\triangle\dot{y})](e^{(-a(\triangle y))-1} & F_y \geq 0 \\ 0 & F_y < 0 \end{cases}$<br>$F_x = \begin{cases} [K(e^{(-a(\triangle y))-1})\frac{B\dot{x}}{(\triangle\dot{y}-0.1)}] & F_x \geq 0 \\ 0 & F_y < 0 \end{cases}$ | K $-$ Stiffness<br>B $-$ Damping<br>a $-$ constant<br>$\triangle x-$ Net horizontal displacement<br>$\triangle y-$ Net vertical displacement<br>$\triangle\dot{x}-$ Horizontal velocity<br>$\triangle\dot{y}-$ Vertical velocity |
| 4. | Pandy et al., 1995 [47] | 2 | $F_y = \begin{cases} 0.5(10^{450(\triangle y)}) - 3000(\dot{y}) & \triangle y \leq 0 \\ 0 & \triangle y < 0 \end{cases}$<br>$F_x = \begin{cases} 0.5(10^{450(\triangle x)}) - 3000(\dot{x}) & \triangle x \leq 0 \\ -0.5(10^{450(\triangle x)}) - 3000(\dot{x}) & \triangle x < 0 \end{cases}$ | K $-$ Stiffness<br>B $-$ Damping<br>$\triangle x-$ Net horizontal displacement<br>$\triangle y-$ Net vertical displacement<br>$\triangle\dot{x}-$ Horizontal velocity<br>$\triangle\dot{y}-$ Vertical velocity |

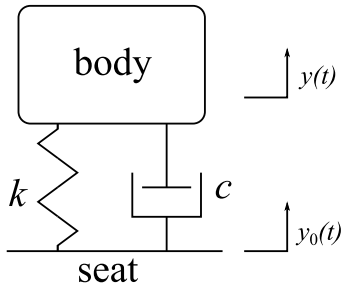


Fig. 29. Representation of the experimental setup for computing the STH transmissibility ratio.

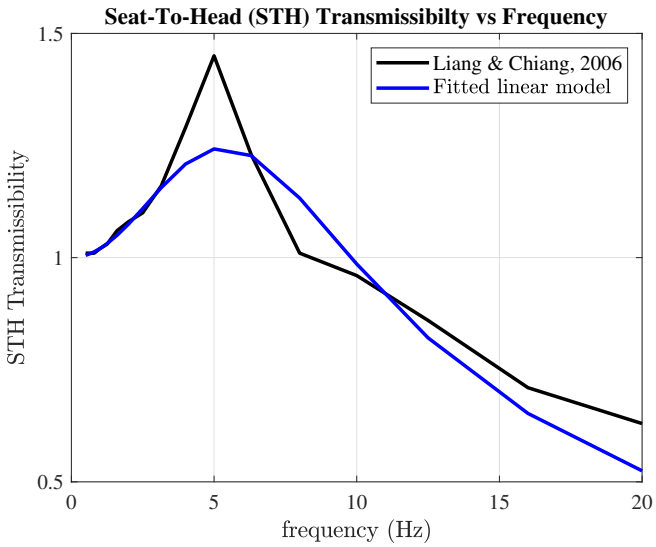


Fig. 30. Plot showing the comparison between the experimental values from literature and fitted model used in the musculoskeletal model.

### *D. Optimisation Algorithm principle*

The optimisation follows 'Covariance Matrix Adaptation Evolution Strategy (CMAES)' algorithm to compute the optimal parameters [31]. The algorithm initially synthesises a population of size $\lambda$ from a normal distribution defined by a mean and standard deviation of each optimisation parameter. Based on this generation, a covariance matrix[3] is formed. Each sample in the population is used to evaluate a particular objective function then. The next generation of the population is then generated by deriving a new mean and standard deviation based on the strongest members of the previous generation. This is done by adapting the new covariance matrix such that the probability of the strongest members occurring in the subsequent generation is increased. This is repeated for each

[3]The Covariance Matrix is a matrix whose element in the *i*, *j* location signifies the covariance between the $i^{th}$ and $j^{th}$ random variable being generated in each population

parameter and the likelihood of the strongest members being generated the subsequent population increases. The CMAES strategy also implements step-size control which decides the length of the subsequent steps, and as a result, guides the optimiser towards the solution.

The optimisation proceeds until either of the following criteria is satisfied.

- The optimisation reaches its maximum number of generations (10000 generations).
- The fitness improves by a very small margin ($10^{-6}$).
- There is no difference in fitness values of the subsequent populations

### *E. SCONE Optimisation to simulation process flow*

The first step in a sequence of steps leading to a simulation of the SiSt task is the loading of the right musculoskeletal model. The control parameters are then initialised using an initial *.par* file. Each optimisation step also generates a *.par* file containing the values of optimisation parameters at that particular step. These parameter files could be simulated to track the progress of the optimisation. Optimisation proceeds until the objective function reaches a minimum value. The final optimised *.par* file is used to generate the simulation in real-time. Executing the simulation generates a *.sto* file containing the joint kinematic amongst other things. This *.sto* file is imported to OpenSim to perform inverse dynamics calculations and derive the joint kinetics. Plots are then generated to visualise the results. Figure 31 illustrates this sequence of actions.

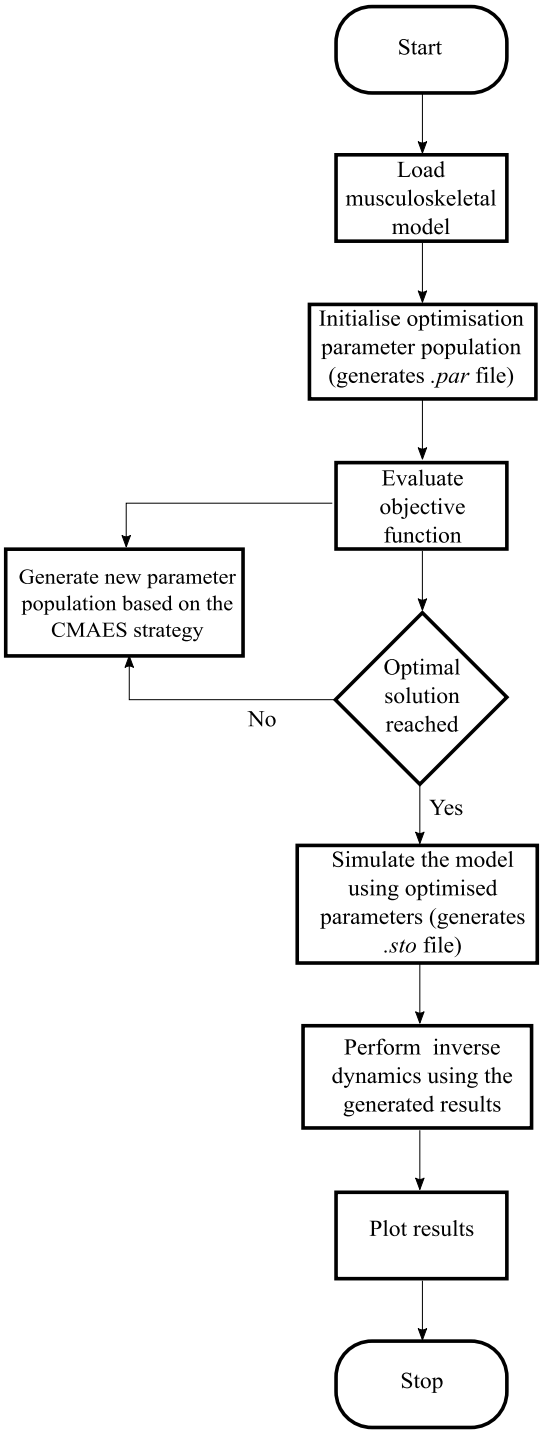


Fig. 31. Flowchart representing the sequence of actions starting from initialising the optimisation setup to generating results.

### *F. Effort term*

The effort term, represented as '$E_{\text{effort}}$' in the objective function, computes the total metabolic energy consumed in the process of sit-to-stand. This term pre-exited in SCONE. Anderson et al., (1999) first composed it [49], Bhargava et al. (2004) detailed it [50] and Wang et al., (2012) later construed it in their study [17]. The metabolic energy expenditure rate of each muscle is computed and summed to represent the total metabolic cost required to perform a particular task. The rate of metabolic energy for each muscle is computed as a sum of five terms which includes heat released as a consequence of the muscle activity and metabolic work rate. This is represented in Equation 18. It should be noted that this Equation and the explanation to this Equation is adapted from Bhargava et al. (2004) [50] and Wang et al., (2012) [17].

$$Effort = \dot{A} + \dot{M} + \dot{S} + \dot{B} + \dot{W} \tag{20}$$

The term $\dot{A}$ is called the activation heat rate, which models the rate of heat energy released as a result of activating a muscle to a certain level of activation. It is a function of the mass of the muscle and level of activation.

The term $\dot{M}$ is called the maintenance heat rate, which models the rate of heat energy released as a consequence of maintaining the muscle contraction at the desired level. In addition to being a function of mass and activation level, it is also a function of the fibre length at the instance it is computed.

The term $\dot{S}$ is called the muscle shortening heat rate, which models the rate of heat energy released as a result of shortening the muscle contraction at an absolute velocity. The rate of heat released as a result of muscle contraction is a function of the total force generated by the musculotendon unit and the shortening velocity of the active contractile element.

The term $\dot{B}$ is called the basal metabolic work rate, which models the basis for computing of the rate of metabolic work. It is a function of the mass of the muscle multiplied by a

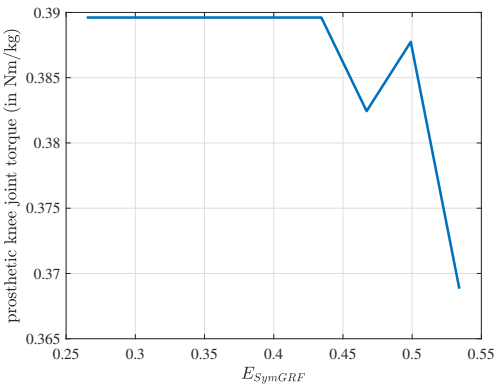


Fig. 32. Plot of peak prosthesis knee torque with respect to the $E_{\text{SymGRF}}$ objective function term

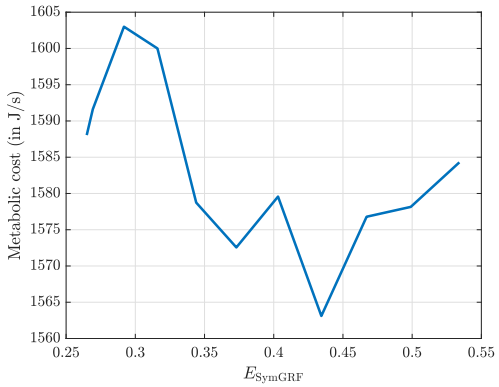


Fig. 33. Plot of the rate of metabolic energy with respect to the $E_{\text{SymGRF}}$ objective function term

factor which is equal to the amount of metabolic energy per unit mass of the muscle for a resting organism at $0^o$ C.

The term $\dot{W}$ is called the positive metabolic work rate. It computes the total rate of positive work produced by the contractile element of the musculotendon unit. It is a function of the force produced and the shortening velocity of the active contractile element.

It should be noted that the effort term computes the above values for only muscle actuators and not other actuators.

### G. Effect of improved weight-bearing on metabolic cost

It was observed from the simulation involving reduced weight-bearing condition that a consequence of utilising 100% of the prosthetic knee's torque (refer Figure 33) capacity leads to an undesirable circumstance of increased metabolic cost. This increased effort is evident from Figure 32, which shows the trend of the effort term with respect to the magnitude of the $E_{\text{SymGRF}}$ term, as the optimisation proceeded towards the optimal solution.

This result of an increase of metabolic cost while the load on the prosthetic limb increases is interesting and noteworthy. In order to perform the SiSt task with minimum energy expenditure, the prosthetic knee must not use its torque capacity to its full potential. Also, trying to load the prosthetic load more than intended does not always lead to the outcome of reduced peak intact knee torque.

### H. Alternate functions to represent muscle excitation signals

An analysis was conducted to deduce an alternate function that could be used to parameterise the muscle excitation signals. The deduced function should adequately bring about the muscle excitations required for the SiSt motion and also have limited parameters to reduce computational effort.

The literature on the SiSt locomotion revealed that the SiSt task is performed with the minimum sum of squared jerk (a derivative of acceleration). Based on a supplementary material in the book by Shadmehr et al., (2004) [51], the displacement function should be a fifth-order differential Equation for a minimum jerk motion which implies that the acceleration should be of the third order. Since the force produced by the muscle is delivered due to the contraction acceleration of the muscle and this acceleration is a linear function of activation signals, it could be concluded that the activation signals are also third order. Since excitation signals and activation signals are of the same order (refer Equation 16) in steady-state, the excitation signal should also be of the third order. Based on this conclusion, a cubic spline could be used to parameterise muscle excitation signals.